doi:10.1016/j.jmb.2003.09.001 *J. Mol. Biol.* (2003) **333**, 1003–1023

JMB

Available online at www.sciencedirect.com

SCIENCE DIRECT®

ELSEVIER

pH-Dependent Amyloid and Protofibril Formation by the ABri Peptide of Familial British Dementia

Rekha Srinivasan[1], Eric M. Jones[2], Keqian Liu[3], Jorge Ghiso[4] Roger E. Marchant[2]* and Michael G. Zagorski[1]*

[1]*Department of Chemistry Case Western Reserve University, 2074 Adelbert Road Millis Science Center Cleveland, OH 44106-7078 USA*

[2]*Department of Biomedical Engineering, Case Western Reserve University, Cleveland OH 44106-7207, USA*

[3]*Department of Biochemistry Case Western Reserve University, Cleveland, OH 44106-4935, USA*

[4]*Department of Pathology, New York University School of Medicine, New York, NY 10016 USA*

**Corresponding authors*

The ABri is a 34 residue peptide that is the major component of amyloid deposits in familial British dementia. In the amyloid deposits, the ABri peptide adopts aggregated β-pleated sheet structures, similar to those formed by the Aβ peptide of Alzheimer's disease and other amyloid forming proteins. As a first step toward elucidating the molecular mechanisms of the β-amyloidosis, we explored the ability of the environmental variables (pH and peptide concentration) to promote β-sheet fibril structures for synthetic ABri peptides. The secondary structures and fibril morphology were characterized in parallel using circular dichroism, atomic force microscopy, negative stain electron microscopy, Congo red, and thioflavin-T fluorescence spectroscopic techniques. As seen with other amyloid proteins, the ABri fibrils had characteristic binding with Congo red and thioflavin-T, and the relative amounts of β-sheet and amyloid fibril-like structures are influenced strongly by pH. In the acidic pH range 3.1–4.3, the ABri peptide adopts almost exclusively random structure and a predominantly monomeric aggregation state, on the basis of analytical ultracentrifugation measurements. At neutral pH, 7.1–7.3, the ABri peptide had limited solubility and produced spherical and amorphous aggregates with predominantly β-sheet secondary structure, whereas at slightly acidic pH, 4.9, spherical aggregates, intermediate-sized protofibrils, and larger-sized mature amyloid fibrils were detected by atomic force microscopy. With aging at pH 4.9, the protofibrils underwent further association and eventually formed mature fibrils. The presence of small amounts of aggregated peptide material or seeds encourage fibril formation at neutral pH, suggesting that generation of such seeds *in vivo* could promote amyloid formation. At slightly basic pH, 9.0, scrambling of the Cys5–Cys22 disulfide bond occurred, which could lead to the formation of covalently linked aggregates. The presence of the protofibrils and the enhanced aggregation at slightly acidic pH is consistent with the behavior of other amyloid-forming proteins, which supports the premise that a common mechanism may be involved in protein misfolding and β-amyloidosis.

Keywords: amyloid; British; fibril; structure; amyloidogenesis

Supplementary data associated with this article can be found at doi: 10.1016/j.jmb.2003.09.001

Abbreviations used: AD, Alzheimer's disease; ABri, British amyloid peptide; AFM, atomic force microscopy; EM, electron microscopy; FBD, familial British dementia; HATU, *N*-[(dimethylamino)-1H-1,2,3-triazolo[4,5-b]pyridino-1-ylmethylene]-*N*-methylmethanaminium hexaflurophosphate *N*-oxide; HFIP, 1,1,1,3,3,3-hexafluoro-2-propanol; MS, mass spectrometry; Th-T, thioflavin-T; TFA, trifluoroacetic acid; WT, wild-type; MALDI-MS, matrix-assisted laser desorption/ionization mass spectrometry.

E-mail addresses of the corresponding authors: rxm4@po.cwru.edu; mxz12@po.cwru.edu

Introduction

Many proteins undergo aberrant folding, and incorrectly fold as non-native structures that either get degraded or persist to form protein aggregates. Such misfolding processes often result in formation of amyloid fibrils (β-amyloidosis), which are insoluble β-pleated sheet structures of distinct tinctorial and morphological properties.[1–3] There are currently 20 proteins that produce amyloid deposits linked to specific human diseases,[4] including the Aβ of Alzheimer's disease (AD), prion of transmissible spongiform encephalopathies, amylin of maturity-onset diabetes, transthyretin of familial amyloidosis, huntingtin of Huntington's disease, and α-synuclein of Parkinson's disease. Although the primary amino acid sequences, molecular sizes, and folded tertiary structures of these proteins are very different, the comparable end-stage fibril structures suggest that some of the amyloid assembly processes may proceed by way of structurally related intermediates and mechanisms. Interestingly, *de novo* designed peptides and other naturally occurring proteins that are not associated with human disease can be induced to form amyloid fibrils, indicating that amyloidosis may be a generic property of all peptides and proteins.[5,6]

The field of protein amyloidosis is under intense investigation. Numerous analytical techniques such as circular dichroism (CD), Fourier transform infrared (FTIR), nuclear magnetic resonance (NMR), negative stain electron microscopy (EM), X-ray fibril diffraction, analytical ultracentrifugation, quasi-elastic light-scattering, size-exclusion chromatography, and atomic force microscopy (AFM) have demonstrated that the soluble amyloid aggregates and the insoluble amyloid plaque cores form unique sizes and fibril morphologies, consistent with cross β-pleated structures. The β-aggregate structures are organized as fibrils of 7–10 nm in diameter, in which the long axis of the fibril is parallel with the helical axis and perpendicular to the β-strands.[7,8] Recent experiments using photoaffinity cross-linking, FTIR and solid-state NMR demonstrated that both parallel and antiparallel β-sheet orientations are present in the amyloid fibrils.[9–11] The amyloid fibrils typically consist of long and unbranched filaments and bind to diagnostic dyes such as thioflavin-T (Th-T) and Congo red.[12,13] Intermediate-like protofibrils that are cytotoxic have been observed[14] and some of the soluble β-aggregrates that precede protofibril formation can act as templates and nucleate or "seed" amyloid formation.[15] Some of these soluble β-aggregrates, such as those from β2-microglobulin, Aβ, and islet amyloid peptide can form membrane pores.[16] The common features of extensive β-sheet aggregates associated with the soluble fibrils that are cytotoxic suggest that the mechanisms of β-amyloidosis for different proteins may involve similar structural pathways.[3,17]

The familial British dementia (FBD) is an autosomal dominant disorder characterized by the presence of amyloid deposits in cerebral blood vessels and brain parenchyma that coexist with neurofibrillary tangles in limbic areas.[18] Patients afflicted with FBD suffer from progressive dementia, spasticity, and cerebellar ataxia, with onset at around the fifth decade of life and full penetrance by age 60. The protein subunit (termed ABri) is the first example of an amyloid molecule created *de novo* by the abolishment of the stop codon in its precursor, which features 266 amino acid residues (BRI-266) and is codified by a single gene, BRI, located on the long arm of chromosome 13.[19,20] The FBD has a single nucleotide change (TGA → AGA, codon 267) that results in an arginine residue substitution for the stop codon in the wild-type (WT) precursor molecule and a longer open reading frame of 277 amino acid residues (BRI-277 instead of BRI-266). The ABri amyloid peptide is formed by the 34 C-terminal amino acid residues of the mutant precursor protein BRI-277, presumably generated from furin-like processing.[21] The ABri has a pyroglutamate N terminus, which is a post-translational modification seen in other brain amyloid proteins such as the Aβ.[22,23] Thus, the point mutation at the stop codon of BRI results in the generation of the 34 residue ABri peptide (instead of the shorter 23 residue WT peptide), which is deposited as amyloid fibrils causing neuronal dysfunction and dementia. Although FBD and AD share almost identical neurofibrillar pathology and neuronal loss that strikingly co-localize with amyloid deposits, the primary sequences of the amyloid proteins (ABri and Aβ) differ. These results support the concept that ABri and Aβ amyloid deposition in the brain can trigger similar neuropathological changes (neuronal loss and dementia) and thus may be a key event in the initiation of neurodegeneration.

Detailed knowledge of the molecular mechanisms associated with ABri amyloidosis is important and could assist in the development of therapeutic approaches for treatment of FBD and other amyloid-related diseases. Earlier biophysical studies established several important facts; notably, that the Cys5–Cys22 intramolecular disulfide bond and the C-terminal extension (Arg24–Asn34) are required for the β-sheet structure formation,[24,25] and that the aggregated ABri peptide induces apoptotic cell death.[26] Here, we extend these preliminary findings and report that the ABri aggregation and protofibril formation are very pH-dependent, as characterized for the first time using AFM studies in air. At neutral pH, only amorphous β-aggregation occurred, without any detectable amyloid fibril formation. Introduction of fibril seeds, generated from ABri solutions at pH 4.9, promoted protofibril formation at neutral pH, suggesting that production of seeds *in vivo* could initiate amyloidosis. The inference of these results in support of a general mechanism of protein amyloidosis is discussed.

Results

Sample preparation

At concentrations of 1–5 mg/ml, purified ABri peptide has limited solubility in aqueous solution at neutral pH. Based on our experience with handling the amyloid Aβ peptide,[27] the insolubility was mostly attributed to the high aggregation state of the dry ABri peptide before dissolution, which presumably results from ABri aggregation in the acetonitrile/water solvent mixture used during the HPLC purification.[27,28] The highly (non-covalent) aggregated or pre-existing "seed" peptides reduce solubility by inducing aggregation, and complicate data interpretation and cause significant lot-to-lot variations, since the quantities of seeds can vary among the peptide batches. To address this issue, as well as obtain a reproducible protocol for handling the ABri peptide, we selected a disaggregation procedure that involved dissolving the ABri peptide at basic pH 9.0, followed by freeze-drying and redissolution in neutral pH buffered solution. Our reason for selecting this protocol was twofold, in that slightly basic pH solutions are extremely successful in disaggregation of the amyloid Aβ peptide,[29] and that a nearly identical procedure had been used to enhance ABri peptide solubility (dissolution in 100 mM Tris buffer at pH 9.0).[24,26]

Although initial experiments showed that at pH 9.0 the ABri was indeed soluble at high concentrations (such as 5 mg/ml), we were concerned that breakage of the Cys5–Cys22 disulfide bond (scrambling) could occur. Numerous studies have established that scrambling is quite rampant at pH 8–10, and often generates covalently linked aggregates through intermolecular disulfide bonding. Representative examples include the 25 residue atrial natriuretic peptide[30] and two tarantula peptides (30 and 35 residues) that inhibit activation of sodium ion channels,[31] which are all of sizes similar to that of the 34 residue ABri. For proteins without free thiol residues (such as the ABri and the above representative peptides), the first step in the scrambling involves β-elimination, where hydroxide ion generates catalytic amounts of proteins with cleaved carbon–sulfur bonds.[32,33] One of the products from this reaction, thiocysteine, decomposes into various thiol groups that subsequently catalyze the formation of intermolecular cross-links and insoluble, high molecular mass aggregates.

To explore the possibility of intermolecular ABri cross-linking, we undertook a study utilizing proteolysis and matrix-assisted laser desorption/ionization time-of-flight (MALDI-TOF) mass spectrometry (MS), similar to procedures previously utilized with the amyloid Aβ peptide.[34] The first objective was to identify peptide fragments that could serve as markers for the scrambling, and the second objective involved analysis of the ABri peptide solutions by looking for the presence or absence of the markers by MS. Proteolytic digestion was carried out with trypsin, which cleaves peptide bonds at the C-terminal sides of Arg and Lys residues. Shown in Figure 1 is a representation of the trypsin cleavage sites in the ABri peptide and the fragments formed after digestion. Scrambling of the Cys5–Cys22 disulfide would produce different intra- and intermolecular peptide fragments (Figure 1(a) and (b)). Fragment **1** forms without scrambling (intramolecular Cys5–Cys22 retention) and results from three cleavages at the peptide bonds connecting Arg9–His10, Lys14–Phe15, and Arg24–Thr25, and corresponds to the observed MS peak at m/z 2129.1. Fragments **2**–**5** form by Cys5–Cys22 scrambling and thus could potentially serve as markers for intermolecular cross-linking. However, fragments **2**, **3**, and **4** could not be utilized as markers, due to either their identical mass with fragment **1** (m/z 2129.1) and/or overlap with matrix cluster peaks.[35] Fragment **5** has a well-resolved MS peak at m/z 2274.8 and accordingly was used to scrutinize for the possibility of inter-molecular cross-linking.

A control digestion with non-disaggregated ABri peptide (dry, aged three months at −20 °C under N_2) did not show a peak at m/z 2274.8, indicating that cross-linking does not occur during storage (Figure 1(c)). With ABri peptide, which was first dissolved in 1,1,1,3,3,3-hexafluro-2-propanol (HFIP) solvent, evaporated to dryness, and then re-dissolved in acetate buffer (pH 4.9), the MS peak at m/z 2274.8 was not present (Figure 1(d)), consistent with the absence of intermolecular disulfide cross-linking. Digestion of aliquots taken from a stock solution in 100 mM Tris–HCl (pH 9.0) showed an MS peak at m/z 2274.8 (Figure 1(e)), establishing that intermolecular cross-linking had taken place. The MS peak is well resolved into five distinct isotopic peaks, thus supporting its identity as a peptide fragment and not the result of a spectral artifact. For the pH 9.0 sample, an additional MS peak at m/z 1139.4 was seen, which corresponds to the thiol-containing fragment Phe15-Ala16-Val17-Glu18-Thr19-Leu20-Ile21-Cys22-Ser23-Arg24 that results from disulfide bond cleavage. These results, which were reproduced three times, clearly establish the proclivity of the Cys5–Cys22 to scrambling at pH 9.0 and that some of the previously reported SDS-stable ABri aggregates may be covalently cross-linked.[24,26]

To ensure that the observed Cys5–Cys22 scrambling was not the result of trace thiol residues in solution,[32,33] perhaps present from small amounts of the reduced ABri peptide (due to incomplete disulfide bond formation), an additional control experiment was performed. In this experiment, latent free thiol groups in a purified ABri peptide sample were alkylated with iodoacetamide,[33,36] followed by re-purification by HPLC. With this peptide, two samples were subjected to digestion by trypsin, one acting as a control (no solution dissolution) while the second

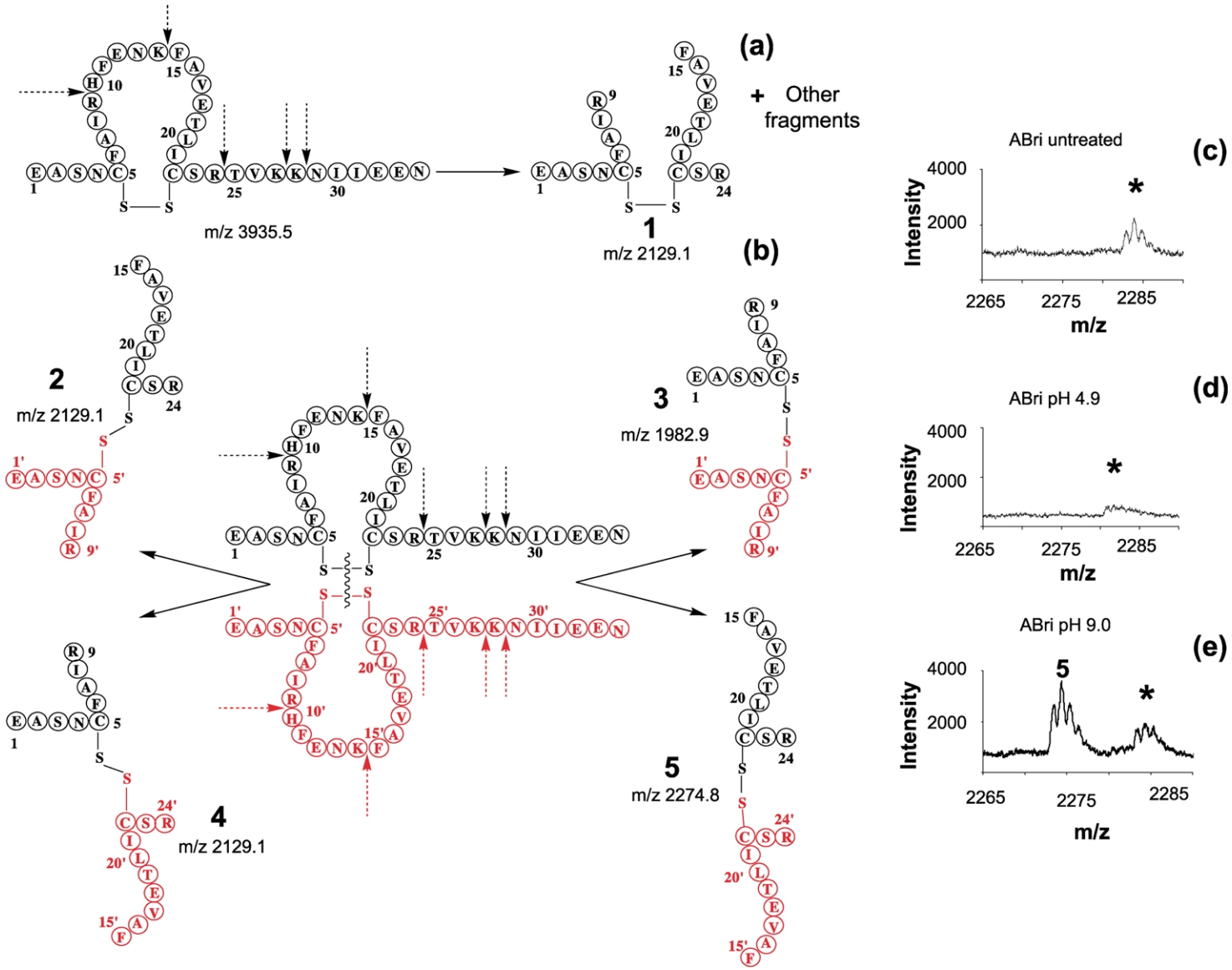

Figure 1 (*legend opposite*)

sample was dissolved in 100 mM Tris–HCl (pH 9.0). The MS analysis of the control sample gave essentially the same results as those with the non-alkylated ABri peptide (Figure 1(c)) and did not show a peak at m/z 2274.8, thus demonstrating that the Cys5–Cys22 remained intact during the reaction with iodoacetamide. For the second sample in pH 9.0 buffer, MS analysis immediately after sample dissolution showed peaks for fragment **5**, as well as the thiol-containing fragment Phe15-Ala16-Val17-Glu18-Thr19-Leu20-Ile21-Cys22-Ser23-Arg24. These latter results are virtually identical with those seen with the non-alkylated ABri peptide, thus establishing that the pH 9.0-induced Cys5–Cys22 scrambling is not caused by trace thiol contaminants.

To address the issue of solubility and obtain consistent results, we thoroughly pre-dissolved the ABri peptide in HFIP solvent and prepared concentrated stock solutions (typically 2 mg/ml) in HFIP from which aliquots were removed and the solvent easily evaporated. For many amyloid-forming proteins, the HFIP promotes disaggregation and generates soluble monomeric structure.[27,37] With storage at 5 °C, the ABri remained soluble in HFIP for several weeks, as shown by reproducible quantitative amino acid analysis. In addition, the above MS data established that the ABri peptide predissolved in HFIP did not undergo scrambling (Cys5–Cys22 remained intact) (Figure 1(d)), unlike that seen in Tris (pH 9.0) buffer solution (Figure 1(e)).

The aggregation state of the ABri peptide was assessed using analytical ultracentrifugation, sedimentation velocity experiments. Because it is not possible to perform these experiments with HFIP solvent, we analyzed fresh 100 μM ABri peptide solutions in acetate buffer at pH 4.3, which are conditions where the peptide shows enhanced solubility.[24,25] The solution was prepared using aliquots taken from ABri peptide stock solutions in HFIP solvent (see Materials and Methods). To avoid problems related to age-induced aggregation, the peptide solutions in acetate buffer were analyzed immediately after sample preparation. As shown in Figure 2, the ABri peptide sedimented as a single boundary, indicating the presence of one predominant aggregation state. Using a single-species fit, analysis of the sedimentation profile afforded a molecular mass of 4200 and a sedimentation coefficient of 0.6 S, consistent with monomeric ABri peptide. These data were reproduced three times, in which the rmsd of the residuals and the fitting was excellent (0.025). Altogether, these data demonstrate that the HFIP solvent is effective in disaggregating the ABri peptide and avoids problems relating to disulfide bond scrambling.

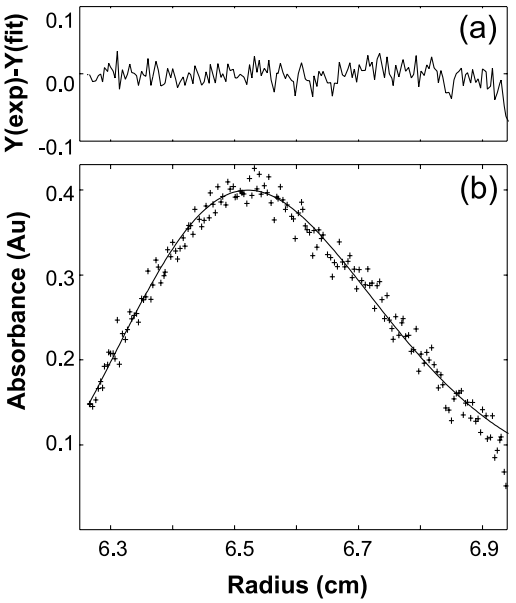

Figure 2. Sedimentation velocity data and a single-species fit for a fresh ABri peptide solution (100 μM, acetate buffer, pH 4.3, 22 °C), as prepared from an HFIP stock solution (see Materials and Methods). (a) The residuals of the fitted function for a single data set. (b) Superimposition of the absorbance data at 235 nm with the fitted function in delta-C mode. The rmsd of the fit is 0.025.

Effects of pH and peptide concentration

The corollary of pH and solution structure was evaluated by CD spectroscopy, a well-established technique for determining protein secondary structure.[38,39] Because CD studies done at 5 °C,

Figure 1. (a) and (b) Summary of the cleavage patterns and peptide fragments resulting from trypsin digestion of the ABri peptide. The structures are not meant to imply that a particular secondary structure or stereochemistry exist about the disulfide bond. The arrowheads show the peptide bond cleavage points that occur at the C-terminal side of the arginine (R) and lysine (K) residues, with analysis of the fragments by MS. (a) Cleavage without Cys5–Cys22 disulfide bond breakage generates the fragment **1** (MS peak at m/z 2129.1), while (b) base-catalyzed disulfide bond Cys5–Cys22 scrambling followed by trypsin cleavage can yield four possible intermolecular recombined fragments **2**, **3**, **4**, and **5** (the diagram shows scrambling between two monomers, one labeled in red and the other in black). (c)–(e) Expanded MS spectral regions of the trypsin digested (1.0 hour incubation followed by quenching) ABri peptide solutions prepared as follows: (c) control solution without HFIP disaggregation, (d) after 0.1 hour incubation in acetate buffer (pH 4.9), and (e) after 0.1 hour incubation in Tris–HCl buffer (pH 9.0). The m/z 2274.8 peak for **5** establishes that Cys5–Cys22 scrambling occurs at pH 9.0, but not at pH 4.9. The peaks labeled with an asterisk (*) are from the trypsin autolysis.

22 °C and 40 °C were nearly identical, we did not further explore the relationship of temperature and secondary structure but restricted measurements to 22 °C. The pH was kept close to the physiologically (neutral) pH, hence varied within the range 4.5–8.9. The initial CD spectra were recorded with the sample in the acidic pH region, with incremental increases of pH. This procedure avoided basic pH ranges (greater than pH 9.0) that could cause Cys5–Cys22 disulfide bond scrambling and cross-linking (see the previous section).

The experiments were designed in a manner to differentiate among three important factors; namely, pH, peptide concentration, and time-dependent (aging) variations, all of which could potentially encourage formation of a particular ABri secondary structure. For example, it is well known that, with β-amyloidosis of other amyloid-forming proteins, higher concentrations of peptide and aging favor production of the aggregated β-sheet structure. For the present work, to discriminate between the pH and peptide concentration-induced structure effects, different concentrations (5, 10, 14, 28, 44 and 56 μM) of ABri were monitored over the pH range 4.5–8.9. The intent of these studies was to establish the presence of β-sheet structure, which is aggregated and, when co-existing with other conformations, should be favored at higher concentrations of peptide. Additional potential inconsistencies that could arise from time-dependent structure variations (i.e. such as the random → β-sheet that occurs with the Aβ[40]) were addressed by obtaining the CD spectral data at identical time-points for all the concentrations of peptide. The CD spectra were recorded within five minutes after each pH re-adjustment, and then re-examined later (one hour and 24 hours) to check for spectral reproducibility.

Shown in Figure 3(a) and (b) are CD spectra for the ABri peptide at 5 μM and 44 μM, respectively. A graphical depiction of the changes in the 198 nm band, as related to peptide concentration and pH, is shown in Figure 3(c). For the lower concentration, 5 μM, at pH 4.5, 5.3, and 6.9 the spectra contain major negative bands centered at 202 nm and no detectable positive band, which is consistent with a predominantly unordered or random structure. Deconvolution of the pH 4.5 spectra using the CDPro algorithm (see Materials and Methods) demonstrated that the conformational weighted average is predominantly random, consistent with visual interpretation. The random structure is characterized by a strong negative CD band at 191–205 nm, where the exact position of the band varies depending on the particular protein system.[39] The intensity of the negative band decreases with increasing pH, indicating that a reduction in random structure is

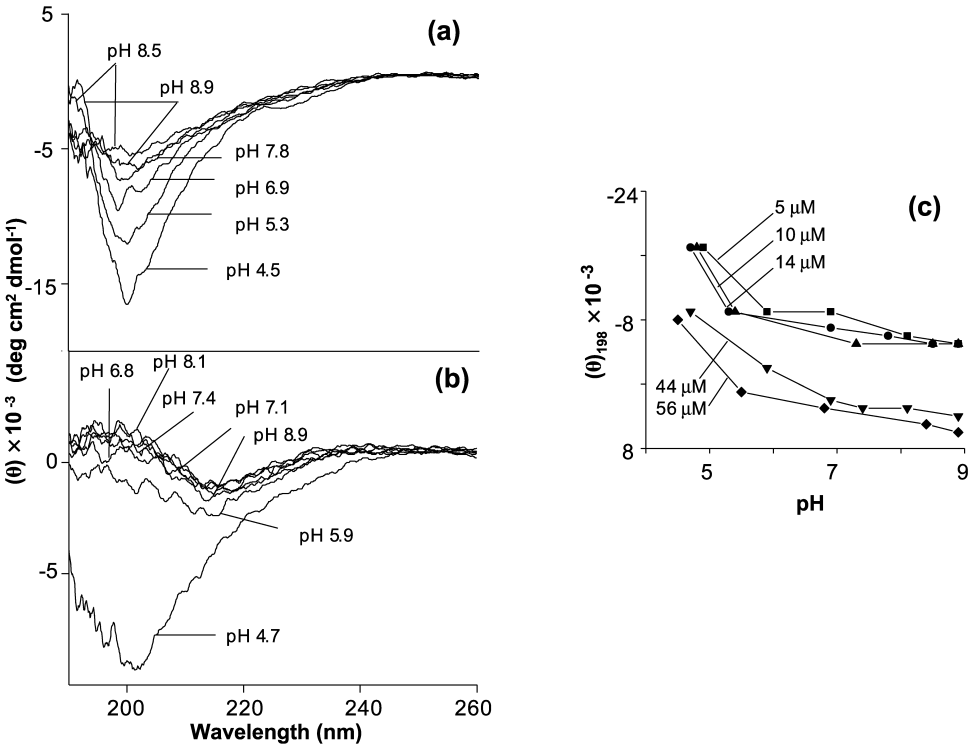

Figure 3. The pH dependent structural changes of the ABri peptide as analyzed by CD, done at 5, 10, 14, 28, 44 and 56 μM ABri and 22 °C. Representative spectra at 5 μM and 44 μM are shown in (a) and (b), respectively, while (c) summarizes the loss in the negative intensity of the 198 nm band (associated with random coil structure) as a function of pH and peptide concentration. The pH was increased in a stepwise manner and the CD spectra were taken within five minutes after each pH adjustment.

occurring (Figure 2(a)). At pH 7.8 and 8.9, the negative bands at 202 nm are barely discernible and are replaced by negative bands at approximately 210 nm and another positive band of comparable magnitude at 195 nm. These latter spectral data conform to a mixture of random and β-sheet structure (the 210 nm value is midway between that of random and β-sheet structure), with an accompanying conformational conversion (random → β-sheet) that takes place during the rise in pH. Another possibility is that the negative band at 202 nm corresponds to a polyproline II structure rather than random structure.[41] However, recent NMR data from our laboratory suggest that the random structure is indeed the major conformation responsible for the 202 nm band (R.S. & M.G.Z., unpublished results).

At higher concentrations (28–56 μM) of peptide, the random → β-sheet conversion occurred more rapidly, as illustrated by the CD data for 44 μM ABri (Figure 3(b)) and the loss in random structure (Figure 3(c)). The negative 202 nm band for random structure is present only at pH 4.7, while the β-sheet is the predominant structure for the remaining pH values. With the exception of pH 5.9, the comparable intensities of positive and negative bands at 195 nm and 217 nm suggest that the conformation is weighted heavily toward β-sheet. Spectral deconvolution using the CDPro algorithm agrees with this interpretation, in that the pH 4.7 data contain little β-sheet (2%) and mostly random (66%) and β-turn (15%), whereas at pH 5.9–8.9 the β-sheet content increases (43–57%) with less random structure (27–29%). The α-helix content is negligible (less than 5%) throughout these studies and is supported by the absence of a band at 222 nm. With aging up to two hours, at pH 5.9–8.9 the 44 μM and 56 μM ABri samples became cloudy and the intensity of the CD bands decreased. As discussed later, analysis of the solutions by EM and AFM revealed the presence of fibrils, some of which were Congo red and Th-T positive, establishing that they are aggregated β-pleated sheet (amyloid-like) structures. Furthermore, because the fibril production lowers the CD-detectable peptide concentration in solution and the corresponding molar-ellipticities, within the pH 5.9–8.4 range the 56 μM concentration may represent the upper limit that can be analyzed accurately by CD spectroscopy.

Together, these data establish that production of the aggregated β-sheet structure is maximized near neutral pH. The lack of a well-defined isodichroic point indicates that more than two conformations may be involved in the random → β-sheet conformational conversion.

Influence of buffer on the ABri secondary structure

The previous sections demonstrated a strong interplay between the pH and the ABri secondary structure, indicating that maintenance of a constant pH during experiments is critical to retain consistency and avoid disulfide bond scrambling. Because the buffer, like the pH, could conceivably affect the distribution of secondary structures,[42,43] we undertook additional studies exploring the effects of different buffers on the ABri secondary structure. A series of buffers were selected with both overlapping and different pH values. To remove the effects of ionic strength that can influence the distribution of secondary structures,[44] the buffers were prepared at concentrations that were sufficient to maintain the desired pH, and keep the ionic strength relatively low and identical for all the buffers ($I = 0.01$ M).[45]

On the basis of the above pH studies, two peptide concentrations were utilized (28 μM and 56 μM), that represent the range where time-dependent changes could occur. Six different buffer solutions were used: two phosphate (pH 6.4 and 7.3), one Tris (pH 8.4), one formate (pH 3.1) and one acetate (pH 4.9). The ABri peptide was aged in the buffer solutions at 22 °C and monitored at different time periods by CD.

In formate (pH 3.1) and acetate (pH 4.9) buffered solutions, the ABri peptide adopts a predominantly random conformation as seen by the minimum band at 202 nm (data not shown), and aging of these solutions for periods up to 336 hours showed no significant conformational changes. However, in phosphate buffer (pH 7.3), the major conformation is β-sheet as shown by a minimum band at 218 nm, while in Tris buffer (pH 8.4) a near baseline spectra indicated the absence of CD-detectable ABri species. The latter two solutions did not reveal any detectable precipitates, but as discussed later, EM and AFM analysis showed amorphous-like aggregates. At higher peptide concentration (56 μM), the CD spectra in formate buffer (pH 3.1) was essentially identical with that at 28 μM, and did not change for time periods up to 336 hours In acetate buffer (pH 4.9) at higher concentrations of ABri (56 μM), the random coil minima moved slightly with aging (202 → 204 nm), indicating that a random → β-sheet conformational conversion may be occurring. Overall, the secondary structures seen in the different buffers largely agree with those obtained without buffer (Figure 2), thus establishing that the buffers exert little influence on the secondary structure.

Fibril formation and morphology

The ABri amyloid fibril structure and morphology were analyzed by negative stain EM and air tapping-mode AFM techniques. To allow systematic comparison with the CD data, solutions with approximately the same pH and peptide concentrations were used. This included preparing two ABri peptide solutions (28 μM and 56 μM) in buffers that had the same ionic strength and incubation times lasting up to 22 days at 22 °C. Because EM is more straightforward, it was first

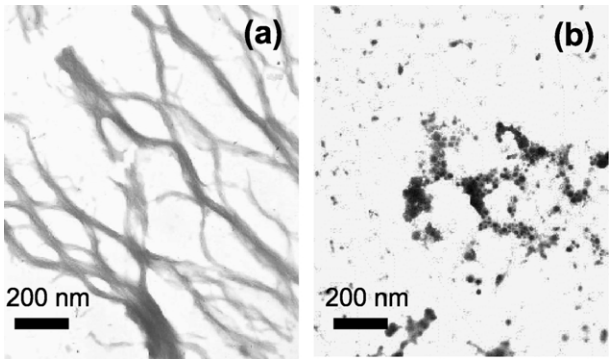

Figure 4. Negatively stained electron micrographs of ABri peptide solutions (28 μM), aged for 14 days at 22 °C: (a) fibrils in acetate buffer (pH 4.9); and (b) amorphous, non-fibrillar aggregates in phosphate buffer (pH 7.3).

used to screen for the presence of fibrils. At different time-points (every one to two days), aliquots were taken from the aggregating solutions and examined by EM and, if needed, examined in greater detail by AFM. All measurements were reproduced three times.

In formate buffer (pH 3.1), the ABri peptide solutions remained optically clear along with the lack of detectable fibrils by EM, in accordance with the random structure seen by CD (Figure 2). By contrast, in acetate (pH 4.9), phosphate (pH 7.3), and Tris (pH 8.4) buffered solutions, the EM data revealed distinct aggregate morphologies, with amyloid-like fibrils at pH 4.9 (Figure 4(a)) and amorphous-like aggregates at pH 7.3 and 8.4 (Figure 4(b)). Production of the aggregates were essentially linear with time, with relatively few seen during the first five days of aging (both of the EM data sets in Figure 4 is after 14 days aging). The results were identical at 28 μM and 56 μM ABri, except that, inevitably, shorter incubation times were required for fibril detection for the higher concentration.

To ascertain that the fibrils seen by EM in acetate (pH 4.9) buffer fold into native β-sheet amyloid-like structures, we used the well-established Th-T and Congo red binding assays.[12,13] Amyloid fibrils show a characteristic interaction with the hetero-aromatic dyes Th-T and Congo red that results in a characteristic spectroscopic response. With binding to the extensive β-sheet network of amyloid fibrils, Congo red shows an increased red-shift in its absorbance spectrum, while Th-T undergoes a characteristic 120 nm red shift of its excitation spectrum that is excited at 450 nm and results in fluorescence emission at 482 nm. As mentioned before, after staining with Congo red, the brain amyloid of FBD patients show the typical yellow–green birefringence under polarized light, supporting the presence of amyloid β-sheet structure.[19]

Using the Th-T binding assay, analysis of five day aged ABri peptide solutions (28 μM) in acetate (pH 4.9) buffer showed maximum fluorescence emission at 482 nm, while analysis of solutions in formate (pH 3.1), phosphate (pH 7.3), and Tris (pH 8.4) buffer showed lower emission levels (Figure 5(a)). The lack of significant Th-T binding at pH 3.1 is consistent with the lack of β-sheet structure seen by CD (Figure 2), and the lack of any detectable fibrils by EM. With the Congo red binding assay, analysis of the ABri peptide solution in acetate buffer (pH 4.9) demonstrated that a shift in the absorbance maximum (485 → 501 nm), and a color change (orange → rose) of the dye were

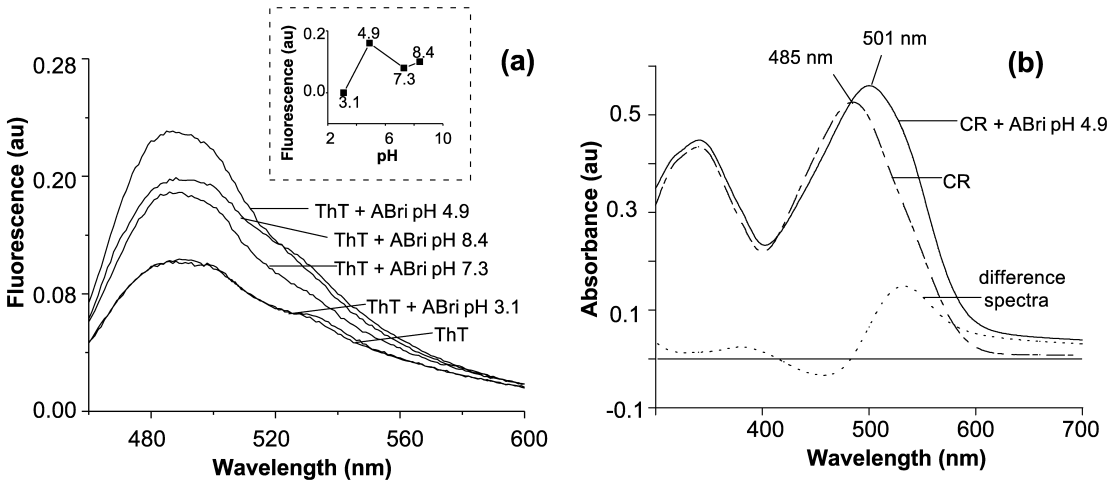

Figure 5. (a) Fluorescence spectra of Th-T alone and mixed with five day aged, ABri peptide (28 μM) solutions at various buffered pH values. A graph of the ABri fluorescence intensity after subtraction from that of Th-T alone lies within the dotted box. Thus, at pH 3.1 there is essentially no Th-T fluorescence enhancement, whereas maximum fluorescence enhancement was seen in acetate (pH 4.9) buffer, consistent with the fibrils observed by EM and AFM. (b) Visible spectral data (300–700 nm) of a mixture of fibrillar ABri peptide and a Congo red dye solution. The characteristic shift in absorbance maximum (485 → 501 nm), as well as the difference spectra (free Congo red-bound Congo red) is indicative of the amyloid-like β-pleated sheet structure. The ABri peptide fibrillar β-aggregates were obtained from a five day aged ABri peptide solution (0.51 mM) in acetate buffer (pH 4.9).

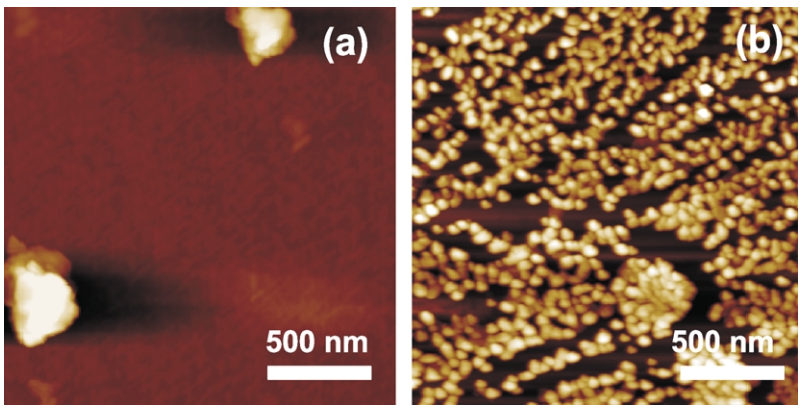

Figure 6. AFM images (1.8 μm × 1.8 μm) of 14 day aged ABri peptide (28 μM) in phosphate buffer (pH 7.3) at 22 °C. The height above the surface and brightness are directly related. (a) Scan area showing the large, irregularly shaped amorphous aggregates (*Z*-range 60 nm), and (b) scan area showing the smaller, spherical aggregates that, over time, assembled into the larger amorphous aggregates (*Z*-range 22 nm). Nearly identical results were seen in Tris buffer (pH 8.4).

noticed in the mixed solution (Figure 5(b)). The absorbance shift is more easily seen by the difference spectrum (free Congo red minus bound Congo red), in support of the amyloid-like β-pleated sheet (Figure 5(b)). Taken together, these data demonstrate that ABri adopts native β-pleated sheet structures characteristic of amyloid fibrils, with formation encouraged in acetate (pH 4.9) buffer.

To examine the morphology at greater resolution, we undertook AFM studies, a well-accepted tool for the analysis of protein surface properties and amyloid fibril structures.[46,47] The height or *z*-dimension was used to estimate the fibril diameters, since the *z*-dimension is generally more accurate and is not affected by the "tip-broadening" effect (see Materials and Methods).[48] Based on differences in the heights, lengths, and periodicities, four distinct morphologies are typically found with most amyloid-forming proteins, and are listed below in order of increasing size: (1) small aggregated species; (2) protofibrils; (3) type 1 mature fibrils; and (4) type 2 mature fibrils.[46,49] The type 1 and type 2 fibrils have distinct morphologies, with the type 1 fibrils having greater heights and distinct periodicities. The type II fibrils have smaller heights and are characterized by a segmented rather than a beaded appearance with less regular dislocations.[46]

For the ABri peptide, the first undertaking was to confirm the observations by EM, which included verifying the absence of amyloid-like fibrils in phosphate (pH 7.3) or Tris (pH 8.4) buffered solutions. The AFM analysis unvaryingly revealed no detectable fibrils, with only amorphous-like aggregates appearing after one day that became more abundant with additional aging. Figure 6(a) shows a representative AFM height image after 14 days aging in phosphate buffer (pH 7.3), where the aggregates are clearly amorphous, based on their asymmetry and large dimensions (100–200 nm width, 50–70 nm height). Besides the larger amorphous aggregates, smaller spherical aggregates (2–8 nm height) were present throughout the images (Figure 6(b)). With aging, the smaller aggregates gradually disappeared and assembled into the larger amorphous aggregates. Type 1 or type 2 mature fibrils were never detected.

The fibrils seen by EM in acetate (pH 4.9) buffer (Figure 5(a)) were next examined with AFM and shown in Figure 7(a) is the image of ABri (28 μM) aged 22 days. The height distribution (Figure 7(b)) indicated that two major types of aggregates are present: (1) smaller spherical aggregates (0.4–1.5 nm height); and (2) larger fibrillar aggregates (1.5–2.2 nm height) that were curved and branched. The spherical aggregates were similar to those seen at neutral pH (Figure 6(b)), except that they were less abundant and smaller. Due to their extensive curvature and branching, the fibrillar aggregates had variable lengths (100–800 nm), but more regular heights (1.5–2.2 nm)

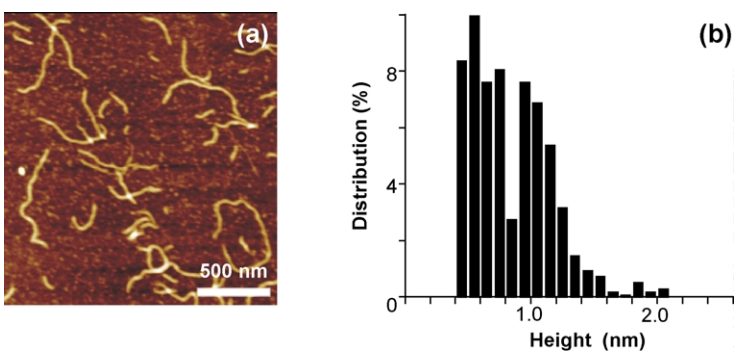

Figure 7. AFM image of 22 day aged ABri peptide (28 μM) in acetate buffer (pH 4.9) at 22 °C. (a) Scan area, 1.8 μm × 1.8 μm (*Z*-range 10.0 nm) and (b) the histogram showing the respective height distribution of all particles observed on multiple horizontal, vertical and diagonal sections taken through the image (0.2 nm data bin).

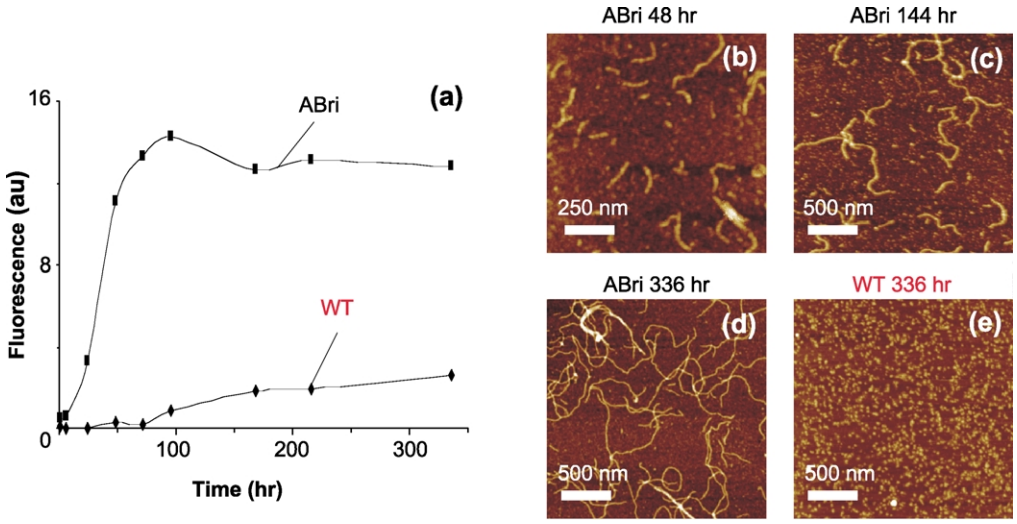

Figure 8. Fibril formation of the 34 residue ABri and 23 residue WT peptides (56 μM) at pH 4.9 and 22 °C, as monitored over time by Th-T and AFM. (a) Graphical depiction of the Th-T fluorescence data (after subtraction from spectra of Th-T alone), which for the ABri peptide shows a short lag phase (six hours) followed by a large enhancement. By contrast, the Th-T data for the WT peptide has a longer lag phase (96 hours) that is accompanied by minimal enhancement. (b)–(d) The AFM images (*Z*-range 10.0 nm) of the ABri peptide at 48 hours (1.0 μm × 1.0 μm scan area), 144 hours (1.8 μm × 1.8 μm scan area), and 336 hours (1.8 μm × 1.8 μm scan area) demonstrate that during the ABri fibrillation the following sequence of events occur: (1) spherical aggregates associate into short protofibrils; (2) spherical aggregates add onto the ends of the short protofibrils forming longer protofibrils; and (3) the long protofibrils are accompanied by the appearance of mature fibrils. (e) Representative AFM image for the WT peptide after aging for 336 hours failed to reveal any fibrils and showed only spherical aggregates.

and periodicities (20–30 nm), both of which are consistent with protofibrils seen with other amyloid-forming proteins.[50–52]

As expected, at higher concentrations of peptide, fibril formation was more rapid, consistent with production of β-sheet aggregates. For comparison, β-aggregation and fibril formation of the shorter WT peptide was monitored alongside with the ABri peptide, with both solutions containing 56 μM peptide in acetate buffer (pH 4.9). During incubation, the two samples were inspected periodically using Th-T and AFM; the Th-T data is shown graphically in Figure 8(a) and representative AFM images are shown in Figure 8(b). The Th-T data clearly demonstrate that WT peptide shows minimal tendency toward producing β-sheet aggregates, whereas the ABri peptide shows rapid enhancement of Th-T fluorescence after a short, six hour lag phase. The AFM also shows that the WT peptide solution failed to produce any amyloid fibril structures, and only small spherical aggregates (Figure 8(e)).

The AFM data of the ABri peptide at higher concentration (56 μM) revealed that several morphological fibril structures are present. When compared to the images obtained at a lower concentration (28 μM) of ABri (Figure 7), the protofibrils were essentially identical, except for slightly greater lengths and the shorter incubation times required for detection. After 48 hours (Figure 8(a)), numerous spherical aggregates (0.5–1.5 nm height) and protofibrils (1.5–2.3 nm height, 250 nm average length) were observed. After 144 hours (Figure 8(b)), the protofibril lengths increased (500 nm average length), while the heights did not change. The heights of the spherical aggregates and the protofibrils were obtained from height distributions through representative images (see Materials and Methods). The data after 336 hours (Figure 8(c)) showed a third type of aggregate, which when compared to the spherical and protofibril aggregates, had distinct morphology (200–800 nm length, 4.0–6.0 nm height) similar to previously reported type 1 mature fibrils for the Aβ peptide.[46] An interesting feature is the extensive curvature and branching of the ABri protofibrils that is retained throughout the aging intervals. Thus, the ABri aggregation occurs through the formation of morphologically distinct aggregates: spherical aggregates, protofibrils, and mature fibrils.

To obtain a more detailed depiction of the protofibrils and their possible association into mature fibrils, higher-resolution AFM images were obtained. Shown in Figure 9(a) and (b) is a single protofibril after six days aging with characteristic height (1.5–2.3 nm) and periodicity (25–32 nm). After 14 days aging, many of the protofibrils became more twisted and laterally intertwined, forming higher-ordered aggregates with greater height (4.0–6.0 nm) and periodicities (37–45 nm), as illustrated by the lateral association of two protofibrils shown in Figure 9(c) and (d). The relative amounts of these coalesced aggregates increased during aging and they eventually produced mature fibrils with greater heights,

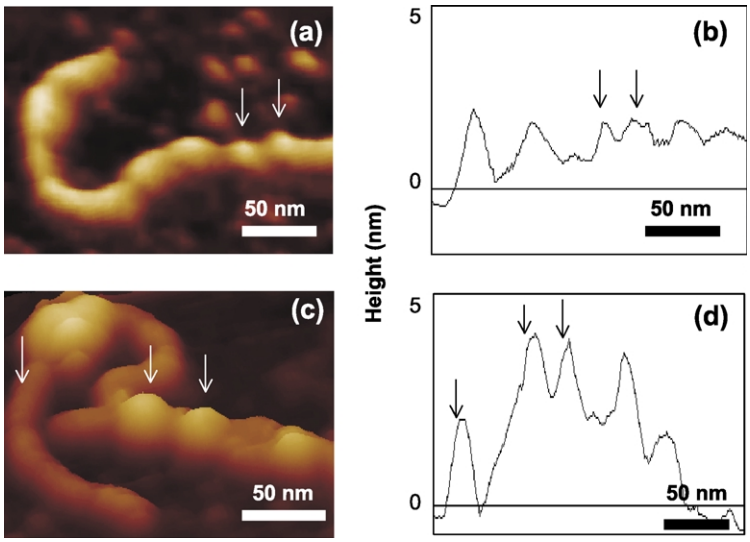

Figure 9. High-magnification AFM images and axial sections of protofibrils, where the arrows in the images (a) and (c) correspond to the arrows in the axial sections (b) and (d), respectively. (a) Single protofibril with the characteristic curvature and the periodic spherical subunits. (b) Axial section across the single protofibril showing the height (*y*-axis, 2 nm) and periodicity (*x*-axis, 25 nm). (c) Image showing the early stages of protofibril association that involves twisting along the axis and production of higher-ordered fibrils. (d) Axial section across the fibrils showing the heights (*y*-axis) and the periodicity (*x*-axis). The arrow at the extreme left in (c) designates a single protofibril (2 nm height), while the other two arrows in (c) show the early stages in mature fibril formation, that consists of two overlapping, twisted protofibrils (4 nm height, 37 nm periodicity). The sample conditions are the same as described in the legend to Figure 8.

periodicities, and dimensions, similar to type 1 mature fibrils.[46] These data demonstrate that during aging the small aggregates assemble into protofibrils and with further aging lead to production of larger mature fibrils.

Seed-induced aggregation at neutral pH

The present results demonstrate that the ABri peptide fibril formation is highly pH-dependent, in that fibrils do not form readily at neutral pH, but do form at modest acid pH. To investigate the possibility that fibrillation at neutral pH could be induced by seeding with previously grown ABri amyloid fibrils, we undertook a series of new experiments. The importance and mechanistic basis of seeding in promoting amyloid fibrillation is well known.[15,53–55]

For this experiment, a freshly prepared ABri peptide solution in phosphate buffer (pH 7.3) was partitioned into three fractions. The first fraction served as a control, while 0.02% and 0.05% seeds were added to the second and third fractions. During incubation at 22 °C, the three solutions were analyzed over time by Th-T and AFM (Figure 10). The control sample (with no seed) showed a constant Th-T fluorescence, which was accompanied by the appearance of amorphous and spherical aggregates by AFM, consistent with previous observations (Figure 6). The seeded reactions were characterized by enhanced Th-T fluorescence, particularly for the sample containing 0.05% ABri seed. For both seeded samples, the AFM data showed amorphous and spherical aggregates, and protofibril structures with dimensions consistent with those produced in acetate buffer (Figures 7–9). The protofibril structures were more abundant in the sample with 0.05% seed, where longer protofibrils were present after 144 hours aging. These data demonstrate that amyloid fibrillation at neutral pH can be initiated by pre-existing amyloid seeds.

The inability of the seeding experiments to generate more mature, elongated fibrils is interesting and could be due to the absence of pre-existing protofibrils in the neutral pH solution, which contains only amorphous and spherical aggregates. This interpretation is consistent with previous studies of the Aβ peptide,[50] in which the rate and efficiency of the (seeded) spherical aggregate → protofibril → mature fibril conversion is highly dependent on the pre-existing fibril content; solutions lacking protofibrils required extended time for detection of mature, elongated fibrils.

Discussion

A growing body of evidence suggests that defects in protein folding and degradation are involved in human disease, particularly neurodegenerative diseases such as the prion-related disorders (i.e. scrapie), AD, Parkinson's disease, and Huntington's disease.[1–3] In all these disorders, proteins accumulate in characteristic lesions in the brain, such as amyloid plaques (Aβ and ABri peptides in AD), Lewy-bodies (α-synuclein in PD), and polyglutamine tracts (huntingtin and ataxin in Huntington's disease). Although it is not known whether the protein aggregates are involved in the disease directly, recent work has shown that species formed early in the aggregation of non-disease-associated proteins can be inherently highly cytotoxic. This finding provides added evidence that avoidance of protein aggregation is crucial for biological function and suggests common features in this family of protein deposition diseases.[17]

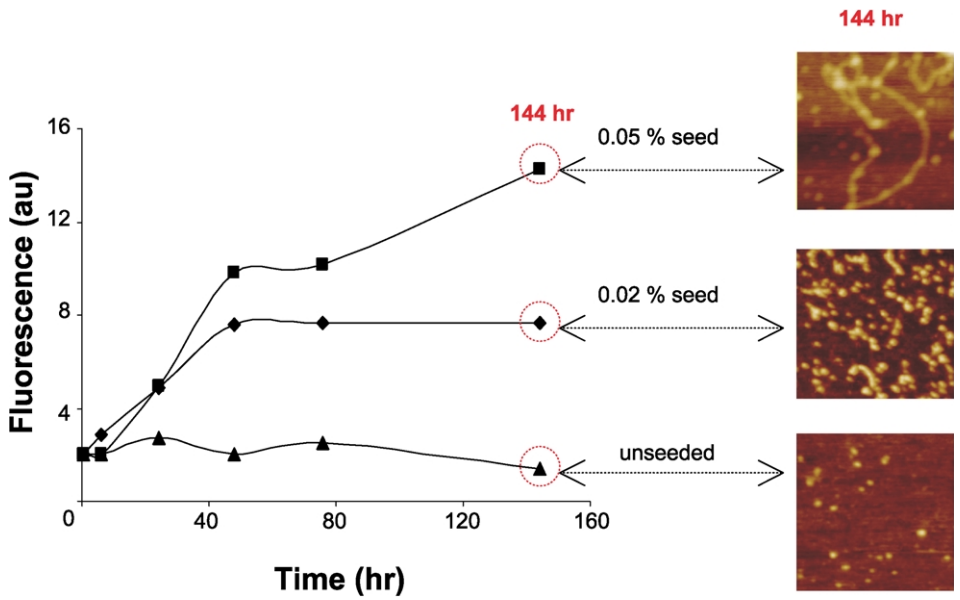

Figure 10. Seed-induced fibril formation of the ABri peptide (20 μM) in phosphate buffer (pH 7.3) at 22 °C. The seeds or pre-existing fibrils were generated from aged ABri peptide (acetate buffer, pH 4.9) and were added as percentage weight fractions (see Materials and Methods). Fibril formation was monitored over time (up to 144 hours) by Th-T fluorescence and AFM for three samples: (1) unseeded-control; (2) with 0.02% seed; and (3) with 0.05% seed. The Th-T spectral data were subtracted from appropriate blank samples, which included Th-T alone, and for samples (2) and (3) phosphate-buffered solutions containing only 0.02% and 0.05% seeds, respectively. The AFM images correspond to samples aged for 144 hours (*Z*-range 10 nm, (400 nm)^2 cross-section). The unseeded sample showed essentially no Th-T fluorescence enhancement with time and only amorphous and spherical aggregates, whereas the seeded solutions show Th-T fluorescence enhancement and numerous protofibril structures.

A major focus of our research is to elucidate the molecular mechanisms associated with amyloid formation. Because recent work has established that the ABri peptide is the major protein component of amyloid deposits in the British kindred, and is capable of activating the complement cascade at levels comparable to those of the Aβ peptide of AD,[56] it constitutes an ideal model to study the relationship among β-aggregation, β-amyloidosis, vascular pathology and neuronal dysfunction. The results presented here demonstrate that the β-aggregation and fibril formation of the ABri peptide are very pH-dependent, and that the β-amyloidosis proceeds by way of a protofibril intermediate. Because these properties exist with other amyloid-forming proteins, the present data support the hypothesis that common mechanisms may be involved in protein β-amyloidosis.

Previously reported biophysical studies of the ABri peptide

Overall, the majority of the present results agree with previously published work, in that the ABri peptide exhibits pH-dependent solubility and a high propensity for β-sheet secondary structure. In the following sections, we briefly highlight the earlier biophysical work and discuss any apparent discrepancies with the data presented herein.

On the basis of negative stain EM, preliminary reports demonstrated that the synthetic ABri peptide formed fibril like aggregates at neutral pH with diameters in the range of 4.0–7.5 nm with extensive branching and curvature.[21] Basically, these fibrils are comparable to those observed by AFM in the present study (4.0–6.0 nm height or diameter), with the exception that our fibrils do not form at neutral pH, but instead at pH 4.9. At neutral pH, the ABri peptide was predominantly amyloid-like β-sheet structure (Figure 2) and eventually precipitated as amorphous (non-fibril) like aggregates. In fact, amyloid fibrils were never detected at neutral pH, despite varying the ABri peptide concentration and regular monitoring of the aggregating solutions by EM and AFM for periods up to 22 days. It may happen that, because the earlier study did not employ any disaggregation procedures,[21] pre-existing seeds that were present in their ABri peptide solutions induced fibril formation, which is supported by the present seeding experiments (Figure 10). In this study, we employed an HFIP-disaggregation protocol that effectively removed any seeds, and thus avoided any problems related to seed induced fibril formation.[15,27,46]

Subsequent reports demonstrated that the ABri peptide was soluble in water at pH 4.3 and Tris–HCl (pH 9.0) buffer, but only sparingly soluble at intermediate and neutral pH values with the major solution conformations being random and β-sheet.[24,25] The overall conclusion from these studies was that the Cys5–Cys22 disulfide bond and the C-terminal extension (Arg24–Asn34) are required to produce β-sheet dimers that undergo further aggregation into fibrils. This same group reported that non-fibrillar aggregates of the ABri peptide are more toxic than the amyloid fibrils.[26]

Basically, the majority of these previous results[24–26] concur with our work regarding the pH-dependent peptide solubility and secondary structures (random and β-sheet). In addition, the lack of EM-detectable fibrils for freshly prepared ABri solutions at neutral pH agrees with the present study. To circumvent problems related to the ABri peptide insolubility, the previous work[24,26] prepared concentrated stock solutions (5 mg/ml) in 100 mM Tris–HCl (pH 9.0) buffer, which were analyzed over a three week period by SDS-PAGE for aggregation and diluted in neutral buffered medium to test for cellular toxicity. Although analysis by electrospray mass spectrometry did not detect covalently linked ABri dimers,[24] this same study revealed that the incubations at pH 9.0 produced SDS stable aggregates, which in our opinion could represent non-physiologically relevant, disulfide cross-linked aggregates.

Our proteolysis experiments established that after trypsin digestion, identically prepared stock solutions contained MS peaks at m/z 1139.4 and 2274.8 (Figure 1(e)) indicative of scrambling of the Cys5–Cys22 disulfide. Moreover, because our MS analysis was done immediately after preparation of the stock solution, it is reasonable to assume that the scrambling would become more prevalent during a three week aging period. The previous work also showed that pretreatment with reducing agents such as 2,3-dihydroxybutane-1,4-dithiol (DTT) prevented detection of the aggregates detected by SDS-PAGE.[24] However, because the SDS generally breaks apart non-covalent aggregates, the high molecular mass aggregates and fibrils seen after incubations at pH 9.0,[24,26] are most-likely covalently cross-linked from scrambling of the Cys5–Cys22 disulfide, and that the DTT broke up the disulfide cross-linkages. It is well known that DTT is very selective in breaking up intermolecular disulfide bonds in multimeric protein aggregates; see work with insulin[32] and the atrial natriuretic peptide.[30]

The likelihood of ABri disulfide-bonded β-sheet aggregates is supported by other CD studies of recombinant reduced ABri (red-ABri) peptide, which lacks the disulfide bond between Cys5 and Cys22.[57] These studies showed that with aging at neutral pH the red-ABri peptide was prone to β-aggregation, as determined by loss of CD signal intensity with concomitant precipitate formation. However, when identical studies were conducted with reducing agents (such as 1 mM cysteine), the CD signal remained constant and there was no peptide precipitation. The implications were that the reducing agents prevented formation disulfide-bonded β-aggregates.[57] It appears that the intermolecular cross-linking of the red-ABri peptide is pH-dependent, since related studies at pH 9.0 did undergo β-aggregation,[24] which is significant, since disulfide bond formation *via* air oxidation is favored strongly above pH 8.0.[32,33]

For the present study, we overcame problems related to the ABri peptide insolubility and disulfide bond scrambling by preparing stock solutions (2 mg/ml) in HFIP solvent (see Materials and Methods). With analytical ultracentrifugation sedimentation velocity techniques, analysis of the freshly prepared aqueous solutions were consistent with a monomeric ABri peptide, thus demonstrating that the HFIP solvent is effective in disaggregating the ABri peptide.

pH-Dependent amyloid formation

The present data show clearly that the solution pH plays an important role in promoting the amyloid-like β-sheet structure and the characteristic fibril morphology. In fact, similar pH-dependent structural (α-helix → β-sheet or random → β-sheet) and morphological changes are shared by other amyloid-forming proteins, such as the Aβ,[40] β2-microglobulin,[58] gelsolin,[59] Vkappa-III Bence Jones protein,[60] HypF N-terminal domain,[61] poly(γ-methyl-L-glutamate)-grafted polyallylamine,[62] transthyretin,[63] α-synuclein,[64] human prion protein,[65] SH3 domain α-subunit of bovine phosphatidylinositol-3′-kinase,[66] and major cold-shock protein.[43,67] With most of these proteins, β-amyloid formation is enhanced at slightly acidic pH values (less than neutral pH) and it is thought that the α-helix → β-sheet or random → β-sheet transitions are early events in the production of the toxic aggregates, including the protofibrils.

In the acidic pH range 3.1–4.3, the ABri peptide adopts almost exclusively random structure, as shown by CD, the lack of Th-T binding and the absence of fibrils as judged by EM and AFM. This interpretation is consistent with the predominantly monomeric structure, as determined by analytical ultracentrifugation (Figure 2). Thus, neutralization of the Glu12, Glu18, Glu32, and Glu33 side-chain negative charges (expected pK_a 4.5) leads to a loss of structure and propensity toward β-aggregation. At neutral and slightly basic pH (pH 7.1–8.3), no distinct fibril morphology was observed, except for smaller spherical aggregates that gradually disappeared and assembled into larger amorphous aggregates. The ABri peptide is only sparingly soluble at neutral pH and, based on the results of CD studies, folds as a β-sheet structure, which was accompanied by decreased signal intensity due to formation of non-CD-detectable aggregates. The lower solubility and rapid precipitation of the ABri peptide at neutral pH may be associated with the proximity to its calculated pI 6.9 (estimated using the ProtParam tool of Expert Protein Analysis System (ExPASy) of the Swiss Institute of Bioinformatics, B., Switzerland†). This suggests that neutralization of the charges prevents formation of a well-defined amyloid fibril structure and that non-specific aggregation processes among the neutral molecules occur, possibly by exposed

† www.expasy.com

hydrophobic surfaces. At pH 4.9, the ABri undergoes a slower and more controlled β-aggregation, where it is possible for fibril formation to occur, similar to the behavior of the amyloid Aβ peptide.[37]

The production of ABri amyloid fibrils at pH 4.9 suggests that protonation of the His10 side-chain (expected pK_a 6.5) plays an important role in maintaining the fibril structure and morphology. Most importantly, the Congo red and Th-T binding establish that the fibrils formed in acetate (pH 4.9) buffer have native amyloid structure, similar to those seen in brain tissue. Other proteins share the relationship of native fibril morphology and pH, including the amyloidogenic light chain variable domain, SMA, which adopts pH-dependent partially folded intermediates that are responsible for different aggregation pathways (amorphous and fibrillar).[68] The protein β2-microglobulin likewise produces discrete amyloid fibril morphologies at different pH values.[69]

The ABri self assembly into amorphous aggregates at pH 7.1–8.3 did not lead to the production of protofibrils or mature fibrils, in contrast to results seen with other proteins such as the amyloid Aβ(1–40) and the SMA.[70,71] However, because the ABri peptide produces amyloid fibrils *in vivo*, this suggests that other micro-environmental changes may be required for β-amyloidosis in the brain.[72] One possibility is that *in vivo* small amounts of partially aggregated (seed) conformers, which may be equilibrating with the monomer, are required to initiate β-amyloidosis, similar to that seen with β2-microglobulin.[73] Production of the seed conformers could be initiated from the binding to metal ions, glycosaminoglycans, or membrane surfaces.[72] Another possibility is that the *in vivo* passage through an acidic biological compartment such as a lysosome induces ABri fibril formation,[58,63] as proposed for the Vkappa-III Bence Jones protein that adopts aggregated fibrillar conformation at mildly acidic pH and aggregated non-fibrillar conformation at neutral pH.[60] Because the main clinical hallmark of FBD is cerebral hemorrhage, not dementia, which is accompanied by amyloid ABri deposits in arterial walls and basement membranes, the interaction of the ABri with biological surfaces and/or acidic micro-environments may be involved in the β-aggregation process. Most significantly, our data demonstrate that ABri fibril seeds do initiate amyloid fibril formation at neutral pH (Figure 10), rather than the amorphous product of the spontaneous reactions (Figure 6). Additional studies exploring the possibility of seed-induced ABri fibril formation are currently underway in our laboratory.

Protofibril as a common intermediate in protein misfolding and β-amyloidosis

In general, the mechanism of protein β-amyloidosis is thought to involve a nucleation-dependent polymerization, which involves formation of a partially structured conformer that is derived from a natively unfolded structure or from the unfolding of a globular-like structure.[55] Once formed, the partially structured conformer undergoes β-aggregation into nuclei or seeds that act as templates in initiating fibril growth.[15,74] Although the detailed mechanisms for such processes are not known, recent information has been gleaned about the steps involved in fibril formation (fibrillation), particularly regarding the protofibril that is thought to be a common intermediate for many amyloid-forming proteins.[14]

For most amyloid-forming proteins, the overall transformation of fibrillation usually follows the pathway: small spherical aggregates → intermediately-sized protofibrils → mature type 1 and type 2 amyloid fibrils.[46,55] Extensive AFM studies suggest that the initially formed spherical aggregates associate linearly to form the protofibrils. The third and fourth species are the mature amyloid fibrils (type 1 and type 2) that posses a common cross β-sheet core with different numbers of protofibrils that are either intertwined into helices or associated side-to-side as twisted ribbon structures.[50,52,75]

The protofibrils normally have three morphological features that are distinct from the mature fibrils: (1) the protofibril sizes are smaller (1–6 nm height or diameter); (2) the lengths are flexible, random curved-linear structures (5–200 nm length); and (3) protofibrils contain characteristic repeat periods or periodicities (20–30 nm) that are shorter than the mature fibrils and similar to beads on a string.[50,51,69] The beaded appearance and periodic repeat result from the linear addition of spherical aggregates.[46] The ABri protofibril heights (1.5–2.3 nm) are slightly smaller than those of other amyloid proteins: Aβ(1–40) 2.8–3.4 nm,[46] Aβ(1–42) 3.6–4.8 nm,[46] amylin 2.4–3.7 nm,[76] β2-microglobulin ~3.5 nm[69] and α-synuclein 4.0–5.0 nm.[77] These differences are due to the amino acid lengths and the presence of the ABri disulfide bond, in that proteins with shorter amino acid lengths and disulfide bonds are more compact and thus have shorter protofibril heights. By contrast, the ABri protofibril lengths (100–800 nm) and periodicities (20–32 nm) are both consistent with the protofibrils seen with other amyloid-forming proteins.

Another interesting observation is lack of any detectable ABri type 2 mature fibrils. Under the experimental conditions (26–56 μM peptide, pH 4.9, 22 °C), the protofibrils and mature fibrils co-exist and, unlike other proteins, do not produce type 2 mature fibrils. Coincidentally, the brains of the British kindred have both non-fibrillar (diffuse) and amyloid plaque fibrils that are more consistent with type 1 than with type 2 fibrils.[18,78] As measured by negative stain EM, the *in vivo* fibrils are crisscrossed (approximately 10 nm), similar to those seen in sporadic AD patients, which have an 8–10 nm diameter and two filament wound

morphology (30–50 nm periodicity) as seen from analysis of plaque material[79,80] and EM studies of tissue sections.[81] Ultrastructural analysis indicates that the amyloid lesions appear as bundles of fibrils, while non-Congo red deposits consist of amorphous electron-dense material with sparsed dispersed fibrils.[78] The fibrillar (type 1-like) ABri deposits are associated with high astrocytic and microglial response.[20] Unlike sporadic AD, the FBD has amyloid plaques in the brain cerebellum and accompanying cerebral ataxia, as well as systemic amyloid deposition in peripheral tissues such as the pancreas and myocardium.

Conclusions

There are three major results from the present studies that could have major implications for understanding the mechanisms associated with protein misfolding and amyloid formation. First, the ABri peptide shows a strong pH-dependence of fibril formation; second, during amyloidosis, the ABri peptide produced protofibrils as intermediates during fibril maturation; and third, ABri fibril seeds may be required to initiate amyloid formation at neutral pH. Because these events have been associated with β-amyloidosis of other proteins, biophysical studies of the ABri peptide may provide insight into unraveling a unifying mechanism coupled with protein misfolding events. The lack of amyloid fibrils at neutral pH suggests that protonation of the His10 side-chain is important in maintaining the amyloid fibril structure.

The observation of ABri protofibrils is especially significant, as numerous studies have established that the protofibrils are neurotoxic by altering the metabolism and electrophysiology of neurons.[82,83] It is thought that stabilization of the protofibril could inhibit the fibril formation and delay the onset of neurodegenaration. More recent evidence suggests that oligomeric and protofibrillar species are potentially toxic, and compounds that inhibit fibril formation or stabilize prefibrillar species are causing a deleterious effect. More detailed biophysical studies exploring the effects of other environmental variables (temperature, peptide concentration, ionic strength) on the fibril structure, as well as other studies involved with identification of the peptide surfaces involved in the small aggregates → intermediate-sized protofibrils → larger amyloid fibrils transformation could lead to the design of specific inhibitors to block the β-aggregation processes of the ABri and other amyloid proteins.

Materials and Methods

Peptide synthesis, intramolecular disulfide bond formation, and purification

The WT and ABri peptides were synthesized, using t-BOC chemistry, by Dr James I. Elliott at the W. M. Keck Protein Chemistry Facility (Yale University), or prepared in our own laboratory on automated synthesizers (model 9050 or 433A, Applied Biosystems). For the latter, the reagents were purchased from commercial sources (PeBiosystems and AnnaSpec), utilizing standard Fmoc protocols with Asn-PEG-PS resin and *N*-[(dimethylamino)-1H-1,2,3-triazolo[4,5-b]pyridino-1-ylmethylene]-*N*-methylmethanaminium hexaflurophosphate *N*-oxide (HATU) as the coupling reagent. The ABri peptide (34 amino acid residues) has the following primary sequence: ^{1}Pyr-^{2}Ala-^{3}Ser-^{4}Asn-^{5}Cys-^{6}Phe-^{7}Ala-^{8}Ile-^{9}Arg-^{10}His-^{11}Phe-^{12}Glu-^{13}Asn-^{14}Lys-^{15}Phe-^{16}Ala-^{17}Val-^{18}Glu-^{19}Thr-^{20}Leu-^{21}Ile-^{22}Cys-^{23}Ser-^{24}Arg-^{25}Thr-^{26}Val-^{27}Lys-^{28}Lys-^{29}Asn-^{30}Ile-^{31}Ile-^{32}Glu-^{33}Glu-^{34}Asn, with a pyroglutamate (Pyr) residue at the N terminus and a disulfide bond between Cys5 and Cys22.[19] The primary sequence of the WT peptide contains Pyr1–Ser23 (23 amino acid residues) of the ABri peptide. The side-chain protecting groups were *t*-butyl for Ser and Thr; triphenylmethyl for Asn, His and Cys; *t*-butyloxycarbonyl for Lys; *t*-butyoxy for Glu; and 2,2,4,6,7-pentamethyldihydrobenzofuran-5-sulfonyl for Arg. Disulfide bond formation was achieved by on-resin oxidation of the peptide with iodine in methanol solution.[84] After synthesis, the resin was swelled in dimethyl formamide (DMF) for 15–20 minutes, after which the DMF was removed by decantation, followed by the addition of more DMF (10 ml) and a drop-wise addition of an iodine in methanol solution (0.3 ml, 0.091 μmol, 300 mM), followed by stirring at room temperature for three hours. After removal of the iodine in methanol solution by decantation, the resin was washed with DMF (3 × 5 ml), dichloromethane (3 × 5 ml) and methanol (3 × 5 ml). Trace amounts of solvents were removed from the resin under reduced pressure (eight hours, 13×10^{-3} bar). The peptide was cleaved from the resin using a mixture of trifluoroacetic acid (TFA)/phenol/water/thioanisole/1,2-ethanedithiol (83:5:5:5:2 by vol.), followed by precipitation and washing repeatedly with diethyl ether. The solvents were removed under reduced pressure and the crude peptide was purified by RP-HPLC (Prosphere 300 C4 semi-preparative column, Alltech) with a solvent gradient consisting of trifluoroacetic acid (TFA)/water/acetonitrile (0.1:95:4.9 → 0.1:5:95 by vol., over a period of 40 minutes). The lyophilized peptides were stored desiccated at −70 °C and the peptide identities were confirmed by MALDI-MS and amino acid analysis. As shown below, the peptides had excellent agreement between the predicted and determined amino acid content: MALDI-MS for the WT peptide m/z 2609.7 and molecular mass excluding the CF_3COO^- salts 2609.9. MALDI-MS for the ABri peptide m/z 3935.3 and molecular mass excluding the CF_3COO^- salts 3935.5. Amino acid analysis for the ABri peptide: Asx 4.1 (4), Thr 1.9 (2), Ser 1.9 (2), Glx 5.0 (5), Ala 3.1 (3), Cys 1.5 (2), Val 2.0 (2), Ile 2.9 (4), Leu 1.1 (1), Phe 3.1 (3), Lys 2.9 (3), His 1.0 (1), Arg 2.0 (2). With the amino acid analysis, the smaller quantity of Ile is presumably due to incomplete hydrolysis of the Ile30–Ile31 bond,[85] which was not investigated further, since the lengthy time required for complete hydrolysis (three to four days) could cause decomposition of the Ser and Thr residues.[85]

Buffer solutions

Six buffer solutions were prepared at constant ionic strength ($I = 0.01$ M),[45] and the final pH was confirmed with a meter (Corning 340) fitted with

micro-combination electrode (Microelectrodes) that was calibrated with pH 4.00, pH 7.00, and pH 10.0 buffers. The buffers included the following: two phosphate (pH 6.4 and 7.3), two Tris (pH 8.4 and pH 8.9), one acetate (pH 4.9), and one formate (pH 3.1) were prepared by combining the appropriate acid and basic solutions.[45] All the reagents were of the highest commercial grade and were used without further purification.

Peptide solutions and disaggregation protocol

The ABri peptide (2.0 mg, 0.43 μmol) was first disaggregated (in a glass vial) by dissolution in 1.0 ml of distilled HFIP (2:1, w/v) with sonication (model SC-101TH, Sonicor) at 25 °C for about 15 minutes, followed by evaporation of the HFIP under a fine stream of dry N_2 gas. These HFIP dissolving and evaporation steps were repeated three times to fully disaggregate the peptide and remove any TFA solvent that adheres to the peptide after HPLC purification. Similar procedures have shown to be effective in disaggregation of the polyglutamine and amyloid Aβ(1–40) peptides.[27,29,86] After the disaggregation, peptide stock solutions were prepared by re-dissolving the peptide (2.0 mg, 0.43 μmol, 0.43 mM) in 1.0 ml of HFIP with storage under a blanket of dry N_2 gas at 5 °C. With these stock solutions, the ABri peptide remained soluble and monomeric for up to four weeks. The aggregation state was established using gel electrophoresis chromatographic techniques previously described for the ABri peptide,[24] which in our case showed only a single band consistent with a molecular mass of the monomeric peptide. As needed, using calibrated Finn-Pipettes (Labsystems), aliquots were removed from the stock solution, placed in glass vials, with evaporation of the HFIP under a stream of dry N_2 gas and final trace amounts removed under vacuum (0.5 mm Hg, two hours). The dry ABri peptide, which coated the glass walls as a waxy-like layer, was dissolved with gentle vortex mixing in doubly distilled water (3.0 ml) for three minutes, frozen (using solid CO_2/ethanol), and lyophilized. The dry peptide now appeared as a white powder and was dissolved in a known amount of water with or without buffer, depending on the study under investigation. Similar disaggregation procedures were employed for the WT peptide.

Analytical ultracentrifugation

Sedimentation velocity experiments used a temperature-controlled Beckman XL-A analytical ultracentrifuge. A double-sector cell, equipped with a 12 mm Epon centerpiece and quartz windows was loaded with 400–420 μl of a freshly prepared ABri peptide sample (100 μM, pH 4.3, acetate buffer). Data were collected at rotor speed of 60,000 rpm in continuous mode at 25 °C, with a step size of 0.003 cm and an absorbance wavelength of 235 nm. A partial specific volume of 0.743 ml/g was estimated from the amino acid sequence and corrected for temperature.[87] The absorbance data were fit using the SVEDBERG program in delta-C mode.[88]

Proteolysis experiments to explore the possibility of Cys5–Cys22 scrambling

Proteolytic digestion was performed with two separate ABri solutions maintained at pH 4.9 and 9.0, using procedures previously employed with the amyloid Aβ peptide.[34] The pH 4.9 solution was prepared by dissolving dried, disaggregated ABri peptide (0.26 mg, 0.056 μmol) in acetate buffer solution (1.0 ml, 10 mM), in which the disaggregated peptide was obtained from an ABri stock solution (0.13 μl, 0.43 mM) in HFIP (see the previous section). The pH 9.0 solution was prepared according to El-Agnaf *et al.*,[24] where ABri peptide (1.0 mg, 0.22 μmol, 1.1 mM) was dissolved in Tris–HCl buffer (0.20 ml, 0.10 M). From the pH 4.9 and 9.0 solutions, aliquots of 15 μl and 0.78 μl were removed, respectively, with the pH 9.0 aliquot diluted to a final volume of 15 μl with 0.10 M Tris–HCl buffer. These fractions were digested with modified sequencing grade trypsin (Promega) (1:5, ABri/trypsin; w/w) in 50 mM NH_4HCO_3 buffer solution (pH 7.8) for 0.16, 1.0 and 24 hours incubation at 37 °C. The digestions were quenched by acidification with 5.0% (v/v) TFA, and analyzed with a Biflex III mass spectrometer (Bruker) with 4-hydroxy-α-cyanocinnamic acid as the matrix. The dilution of the pH 9.0 aliquot was required to ensure that the ABri concentrations (3.9 μg, 56 μM) were the same for the pH 4.9 and 9.0 solutions before the digestion. Control digestions were carried out with non-disaggregated (no HFIP predissolution) ABri peptide (3.9 μg, 56 μM) dissolved in 15 μl of 50 mM NH_4HCO_3 buffer solution (pH 7.8), and with ABri peptide that was pretreated with iodoacetamide to alkylate any pre-existing thiol impurities. For this latter procedure, the ABri peptide (1.0 mg, 0.22 μmol, 0.11 mM) was dissolved in a NH_4HCO_3 buffer solution (2 ml, 50 mM, pH 8.0), followed by the addition of 50 μl of a 65 mM iodoacetamide (0.6 mg, 3.2 μmol) solution in NH_4HCO_3 buffer (50 mM, pH 8.0).[36] The mixture was shaken at room temperature for one hour, after which the ABri peptide was purified by HPLC and then disaggregated by dissolution in HFIP solvent.

Circular dichroism spectroscopy

Spectra were recorded on a J-810 spectropolarimeter (Jasco) over the wavelength range of 190–260 nm at a scan-rate of 100 nm/minute and a band-width of 1 nm. Depending upon whether a concentrated or dilute peptide solution was measured, quartz cells of 0.02 cm, 0.1 cm, or 1 cm path lengths (Hellma) were used. The CD data (in mdeg) were converted to mean residue molar ellipticity [θ] (deg cm^2 dmol^{-1}) by using:

$$[\theta] = ([\theta]\lambda \times \mathrm{MR})/(10 \times l \times c)$$

where θλ corresponds to the observed ellipticity (mdeg), MR is the mean residue mass (molecular mass of the protein divided by the number of amino acid residues, 115.8 for ABri), l is the optical path length (in cm), and c is the final protein concentration (in mg/ml). No filtering or smoothing techniques were used to reduce noise levels in the spectra, and peptide concentrations were determined by quantitative amino acid analysis. The conformational weights of the secondary structures were determined by using CDPro software, which is a suite of three programs for CD analysis, namely SELCON3, CONTIN, CDSSTTR, and a basis set of 43 reference proteins.[89] The relative amounts of α-helix and β-sheet were obtained from summing together the contributions from helix1 and helix2, strand1 and strand2, respectively, whereas those for β-turn and random structure were read directly from the output.

For the CD studies in the different buffer solutions of constant ionic strength ($I = 0.01$ M),[45] two ABri peptide concentrations (28 μM and 56 μM) were analyzed for each of the following six buffers: two phosphate (pH 6.4

and 7.3), two Tris (pH 8.4 and 8.9), one formate (pH 3.1) and one acetate (pH 4.9), while for the study exploring the effect of pH on the secondary structure, six different peptide concentrations (5.0, 10, 14, 28, 44 and 56 μM) were used. For the latter study, which was done without buffer, the disaggregated and dried peptide (taken and dried from an HFIP stock) was dissolved in doubly distilled water and the initial pH value was usually 3.8–4.2. The subsequent higher incremental pH values were obtained by adding microliter amounts of dilute base (0.10 M NaOH), and the pH values were measured with a pH meter (Corning 340) equipped with an electrode (model MI-412, Microelectrodes). In general, 5–6 pH values were done for each concentration of peptide and the CD spectrum was measured within five minutes after the pH readjustment, and then re-examined by CD (one to two hours later) to check for reproducibility and any spectral changes that may occur over time. To ensure that the addition of the small amounts of dilute base did not alter the peptide concentration, quantitative amino acid analysis was performed at the beginning and end of the study for all five samples, which established that the peptide concentrations remained essentially unchanged (±5%).

Congo red binding

In general, the procedure described by Klunk *et al.*[13] was followed, but with minor modifications. A Congo red stock solution (0.30 mM) was prepared in PBS/ethanol (9:1, v/v) at pH 7.4 and filtered to remove micelles. From this stock solution, a second, diluted Congo red solution was prepared (9.2 μM), for which an accurate concentration was determined by absorbance spectroscopy at 505 nm and a standard Beer–Lambert plot ($\in = 5.53 \times 10^4$ (absorbance unit) $cm^{-1}\,M^{-1}$). Aliquots (25 μl) taken from a five day aged ABri peptide solution (0.43 mM) in acetate buffer at pH 4.9 were combined with 1.0 ml of the Congo red solution (9.2 μM), and incubated at room temperature for 15 minutes. Congo red binding was ascertained by measurement at 300–700 nm using a Lambda 35 UV spectrophotometer (Perkin–Elmer), with subtraction of the baseline spectrum of the phosphate buffer. The absorbance spectrum of (bound) Congo red plus peptide was corrected for the light-scattering by subtracting the absorbance spectra of ABri taken over the visible region. The final spectra were then compared to that of non-bonded Congo red solution (9.2 μM).

Thioflavin-T binding

The Th-T fluorescence measurements were performed on a SLM Aminco spectrophotometer, using excitation and emission slit-widths of 5 nm. For the Th-T binding analysis, fluorescence intensity was measured at different excitation (450 nm) and emission (460–600 nm) wavelengths.[12] At specific time-points, aliquots (20 μl) of ABri peptide solutions (28–56 μM) in formate (pH 3.1), acetate (pH 4.9), phosphate (pH 7.3), and Tris (pH 8.4) were mixed thoroughly with a Th-T solution (0.48 ml, 10 μM) containing potassium phosphate buffer (50 mM, pH 6.0), with immediate measurement of the fluorescence.

Electron microscopy

Aliquots (5.0 μl) of ABri peptide solutions (28–56 μM) containing fibrils were applied to 400-mesh, glow-discharged, carbon-coated copper grids (Electron Microscopes) and left on the grid for 30 seconds at room temperature. Excess solvent was removed from the grid by blotting with a filter paper (Whatman), and the remaining samples were negatively stained by the addition of a 2% (w/v) uranyl acetate solution (5.0 μl) for 30 seconds. The grids were blotted again with filter paper and air-dried before analysis. Using an acceleration voltage of 80 kV, the grids were visualized with a transmission electron microscope (model JEM-100C, Jeol).

Atomic force microscopy

The ABri specimens were prepared for AFM imaging using the well-established methods developed for other amyloid-forming peptides.[46,47,90] Two ABri peptide concentrations (28 μM and 56 μM) were analyzed in the following six buffers: phosphate (pH 7.3), Tris (pH 8.3), formate (pH 3.1) and acetate (pH 4.9). The solutions were left undisturbed at 22 °C for periods up to 22 days, except for slight mixing prior to removal of aliquots for AFM analysis. Previous studies with the amyloid Aβ peptide demonstrated that constant stirring or vortex mixing encourages formation of large aggregates and makes AFM sample preparations less reproducible.[46] The aliquots (10 μl) were applied to the surface of freshly cleaved muscovite mica and left at room temperature for 60 seconds. Next, the mica substrate was tilted, with the lower edge in contact with an absorbant material, and the surface rinsed with water (2 × 50 μl) to remove loosely bound protein, and then blown dry under a stream of N_2 gas. The sample was imaged immediately using a Nanoscope IIIa controller (Digital Instruments) with a Multimode scanning probe microscope. To minimize lateral forces, which can deform the sample and distort the images, all measurements were carried out in the TappingMode™ under ambient conditions using etched, single-beam silicon cantilevers (125 μm length) and a nominal spring constant (20–100 $N\,m^{-1}$), according to the manufacturer's specifications (Digital Instruments). The scanning and feedback control parameters were within the following ranges: RMS drive amplitude 30–300 mV, set point amplitude 0.5–1.2 V, drive frequency 270–300 kHz, and a scan-rate of 1–2 Hz. Prior to imaging, the probe tip was checked carefully for contamination by analysis of the force calibration curve, which usually showed no contamination. When contamination was present (less than 10%), the probe was removed from the instrument, washed with solvents (in the order water, methanol, ethanol, water), blown dry with a stream of N_2 gas, and replaced. The parameters were selected to minimize force that could be applied to the sample without disengaging the tip from the surface. Because the force exerted by the tip on the surface is proportional to the ratio of drive amplitude to set point amplitude, the drive amplitude was set concomitantly with drive frequency in most experiments, and the set point amplitude was adjusted to a level just low enough that the tip remained engaged. In doing so, tip damage and sample deformation were avoided by tapping gently. Gain settings were adjusted to obtain stable images of high resolution. Height distribution for the images were obtained from analysis of horizontal, vertical and diagonal cross sections (ten sections, each containing 512 points), which ensured that a fair height distribution representative of the entire image was constructed. The data from the cross sections were

consolidated into histograms with the data bin set to 0.20 nm. Because the mica surface contributes to the histogram distribution (maximum value 0.40 nm), values exceeding 0.4 nm can be attributed only to the ABri fibrils. It is important to note that the lateral dimensions of objects in a high-resolution AFM image will be exacerbated in the x and y dimension due to the finite size of the probe tip ("tip-broadening effect").[48] Because the z-dimension is not affected by the finite tip size, the height gives a more accurate measurement of the diameter (or thickness) than does the width (x–y dimensions), and thus the heights rather than the widths were used to provide estimates of the ABri fibril diameters.

Seeding experiments

Solutions containing seeds or preaggregated material were prepared by allowing the ABri peptide (1.0 mg, 0.22 μmol) to age at 22 °C in acetate buffer (2 ml, pH 4.9) for 72 hours. The presence of sufficient quantities of soluble, aggregated material was verified by Th-T fluorescence, which showed a maximum signal after 72 hours of aging. This solution was vortex mixed, and aliquots were removed and immediately mixed with freshly prepared ABri peptide solutions (20 μM, phosphate buffer, pH 7.3). The amount of seed added to the reaction mixture was estimated as a weight fraction or molar equivalent of monomeric ABri compared to the ABri in the reaction.[53] The amount of seed present in the final reaction mixture is reported as a percentage (molar equivalent ABri seed/molar equivalent ABri total × 100). The aggregation was monitored over time by Th-T fluorescence and AFM. The Th-T spectral data were subtracted from appropriate blank samples in phosphate buffer, including Th-T alone and solutions containing only seeds.

Acknowledgements

This work was supported, in part, by grants from NIH (AG-14363-04 to M.G.Z.; HL-40047-12, HL-47300-05 and HL-70263-01 to R.E.M.; S10-RR14919, M. D. Barkley) the American Health Assistance Foundation (A2000-056 to M.G.Z.), and the Alzheimer's Association (IIRG-02-4384 to M.G.Z.). We thank David Vanik, Clemens Burda, Anna Samia, Liming Hou, Krisztina Bencze, Mihaela Apetri, Kathy Howard, Vernon Anderson, and Witold Surewicz for helpful discussions, Shu Guang Chen for mass spectrometry measurements, Brian Austen for advice about HPLC purification of the ABri, and John Philo for help with the SVEDBERG program that was for interpretation of the sedimentation velocity data. We are extremely grateful to McHardy M. Smith for providing a preprint of work about disulfide bond scrambling of native inhibitory cystine knot peptides.

References

1. Lansbury, P. T. & Kosik, K. S. (2000). Neurodegeneration: new clues on inclusions. *Chem. Biol.* **7**, R9–R12.
2. Dobson, C. M. (2001). The structural basis of protein folding and its links with human disease. *Philos. Trans. Roy. ser. B*, **356**, 133–145.
3. Temussi, P. A., Masino, L. & Pastore, A. (2003). From Alzheimer to Huntington: why is a structural understanding so difficult? *EMBO J.* **22**, 355–361.
4. Westermark, P., Benson, M. D., Buxbaum, J. N., Cohen, A. S., Frangione, B., Ikeda, S. *et al.* (2002). Amyloid fibril protein nomenclature. *Amyloid*, **9**, 197–200.
5. Chiti, F., Webster, P., Taddei, N., Clark, A., Stefani, M., Ramponi, G. & Dobson, C. M. (1999). Designing conditions for *in vitro* formation of amyloid protofilaments and fibrils. *Proc. Natl Acad. Sci. USA*, **96**, 3590–3594.
6. Takahashi, Y., Ueno, A. & Mihara, H. (2000). Mutational analysis of designed peptides that undergo structural transition from alpha helix to beta sheet and amyloid fibril formation. *Struct. Fold. Des.* **8**, 915–925.
7. Inouye, H., Fraser, P. E. & Kirschner, D. A. (1993). Structure of β-crystallite assemblies formed by Alzheimer β-amyloid protein analogues: analysis by X-ray diffraction. *Biophys. J.* **64**, 502–519.
8. Sunde, M., Serpell, L. C., Bartlam, M., Fraser, P. E., Pepys, M. B. & Blake, C. C. (1997). Common core structure of amyloid fibrils by synchrotron X-ray diffraction. *J. Mol. Biol.* **273**, 729–739.
9. Benzinger, T. L., Gregory, D. M., Burkoth, T. S., Miller-Auer, H., Lynn, D. G., Botto, R. E. & Meredith, S. C. (2000). Two-dimensional structure of beta-amyloid(10–35) fibrils. *Biochemistry*, **39**, 3491–3499.
10. Bouchard, M., Zurdo, J., Nettleton, E. J., Dobson, C. M. & Robinson, C. V. (2000). Formation of insulin amyloid fibrils followed by FTIR simultaneously with CD and electron microscopy. *Protein Sci.* **9**, 1960–1967.
11. Egnaczyk, G. F., Greis, K. D., Stimson, E. R. & Maggio, J. E. (2001). Photoaffinity cross-linking of Alzheimer's disease amyloid fibrils reveals interstrand contact regions between assembled beta-amyloid peptide subunits. *Biochemistry*, **40**, 11706–11714.
12. LeVine, H. (1995). Thioflavine T interaction with amyloid β-sheet structures. *Amyloid: Int. J. Expt. Clin. Invest.* **2**, 1–6.
13. Klunk, W. E., Jacob, R. F. & Mason, R. P. (1999). Quantifying amyloid by Congo red spectral shift assay. *Methods Enzymol.* **309**, 285–305.
14. Haass, C. & Steiner, H. (2001). Protofibrils, the unifying toxic molecule of neurodegenerative disorders? *Nature Neurosci.* **4**, 859–860.
15. Harper, J. D. & Lansbury, P. T. (1997). Models of amyloid seeding in Alzheimer's disease and scrapie: mechanistic truths and physiological consequences of the time-dependent solubility of amyloid proteins. *Annu. Rev. Biochem.* **66**, 385–407.
16. Hirakura, Y., Yiu, W., Yamamoto, A. & Kagan, B. (2000). Amyloid peptide channels: blockade by zinc and inhibition by Congo red (amyloid channel block). *Amyloid: Int. J. Expt. Clin. Invest.* **7**, 194–199.
17. Bucciantini, M., Giannoni, E., Chiti, F., Baroni, F., Formigli, L., Zurdo, J. *et al.* (2002). Inherent toxicity of aggregates implies a common mechanism for protein misfolding diseases. *Nature*, **416**, 507–511.
18. Plant, G. T., Revesz, T., Barnard, R. O., Harding, A. E. & Gautier-Smith, P. C. (1990). Familial cerebral amyloid angiopathy with nonneuritic amyloid plaque formation. *Brain*, **113**, 721–747.
19. Vidal, R., Frangione, B., Rostagno, A., Mead, S.,

Revesz, T., Plant, G. & Ghiso, J. (1999). A stop-codon mutation in the *BRI* gene associated with familial British dementia. *Nature*, **399**, 776–781.
20. Ghiso, J., Holton, J., Miravalle, L., Calero, M., Lashley, T., Vidal, R. *et al.* (2001). Systemic amyloid deposits in familial British dementia. *J. Biol. Chem.* **276**, 43909–43914.
21. Kim, S. H., Wang, R., Gordon, D. J., Bass, J., Steiner, D. F., Lynn, D. G. *et al.* (1999). Furin mediates enhanced production of fibrillogenic ABri peptides in familial British dementia. *Nature Neurosci.* **2**, 984–988.
22. Mori, H., Takio, K., Ogawara, M. & Selkoe, D. J. (1992). Mass spectrometry of purified amyloid beta protein in Alzheimer's disease. *J. Biol. Chem.* **267**, 17082–17086.
23. Tekirian, T. L., Saido, T. C., Markesbery, W. R., Russell, M. J., Wekstein, D. R., Patel, E. & Geddes, J. W. (1998). N-terminal heterogeneity of parenchymal and cerebrovascular Abeta deposits. *J. Neuropathol. Expt. Neurol.* **57**, 76–94.
24. El-Agnaf, O. M., Sheridan, J. M., Sidera, C., Siligardi, G., Hussain, R., Haris, P. I. & Austen, B. M. (2001). Effect of the disulfide bridge and the C-terminal extension on the oligomerization of the amyloid peptide ABri implicated in familial British dementia. *Biochemistry*, **40**, 3449–3457.
25. Lelyveld, V., El-Agnaf, O. M., Siligardi, G., Hussain, R., Haris, P. I., Lee, M. & Austen, B. (2001). Conformational analysis of peptides derived from the *BRI* gene. *Spectroscopy*, **15**, 129–139.
26. El-Agnaf, O. M., Nagala, S., Patel, B. P. & Austen, B. M. (2001). Non-fibrillar oligomeric species of the amyloid ABri Peptide, implicated in familial British dementia, are more potent at inducing apoptotic cell death than protofibrils or mature fibrils. *J. Mol. Biol.* **310**, 157–168.
27. Zagorski, M. G., Yang, J., Shao, H., Ma, K., Zeng, H. & Hong, A. (1999). Methodological and chemical factors affecting amyloid β-peptide amyloidogenicity. In Amyloid, Prions, and Other Protein Aggregates (Wetzel, R., ed.), vol. 309, pp. 189–204, Academic Press, New York.
28. Shen, C.-L. & Murphy, R. M. (1995). Solvent effects on self-assembly of β-amyloid peptide. *Biophys. J.* **69**, 640–651.
29. Fezoui, Y., Hartley, D., Harper, J., Khurana, R., Walsh, D., Condron, M. *et al.* (2000). An improved method of preparing the amyloid β-protein for fibrillogenesis and neurotoxicity experiments. *Amyloid: Int. J. Expt. Clin. Invest.* **7**, 166–178.
30. Wu, S. L., Leung, D., Tretyakov, L., Hu, J., Guzzetta, A. & Wang, Y. J. (2000). The formation and mechanism of multimerization in a freeze-dried peptide. *Int. J. Pharmacol.* **200**, 1–16.
31. Middleton, R. E., Warren, V. A., Kraus, R. L., Hwang, J. C., Liu, C. J., Dai, G. *et al.* (2002). Two tarantula peptides inhibit activation of multiple sodium channels. *Biochemistry*, **41**, 14734–14747.
32. Costantino, H. R., Langer, R. & Klibanov, A. M. (1994). Solid-phase aggregation of proteins under pharmaceutically relevant conditions. *J. Pharm. Sci.* **83**, 1662–1669.
33. Darby, N. & Creighton, T. E. (1997). Probing protein folding and stability using disulfide bonds. *Mol. Biotechnol.* **7**, 57–77.
34. Kheterpal, I., Williams, A., Murphy, C., Bledsoe, B. & Wetzel, R. (2001). Structural features of the Aβ amyloid fibril elucidated by limited proteolysis. *Biochemistry*, **40**, 11757–11767.
35. Keller, B. O. & Li, L. (2000). Discerning matrix-cluster peaks in matrix-assisted laser desorption/ionization time-of-flight mass spectra of dilute peptide mixtures. *J. Am. Soc. Mass Spectrom.* **11**, 88–93.
36. Glocker, M. O., Arbogast, B. & Deinzer, M. L. (1995). Characterization of disulfide linkages and disulfide bond scrambling in recombinant human macrophage-colony-stimulating factor by fast-atom-bombardment mass-spectrometry of enzymatic digests. *J. Am. Soc. Mass Spectrom.* **6**, 638–643.
37. Wood, S. J., Maleeff, B., Hart, T. & Wetzel, R. (1996). Physical, morphological and functional differences between pH 5.8 and 7.4 aggregates of the Alzheimer's amyloid peptide Aβ. *J. Mol. Biol.* **256**, 870–877.
38. Greenfield, N. & Fasman, G. D. (1969). Computed circular dichroism spectra for the evaluation of protein conformation. *Biochemistry*, **8**, 4108–4116.
39. Woody, R. W. (1994). *Circular dichroism of peptides and proteins* Circular Dichroism, Principles and Applications (Nakanishi, K., Berova, N. & Woody, R. W., eds), pp. 473–496, VCH Publishers, New York chapt. 17.
40. Barrow, C. J., Yasuda, A., Kenny, P. T. M. & Zagorski, M. G. (1992). Solution conformations and aggregational properties of synthetic amyloid β-peptides of Alzheimer's disease. Analysis of circular dichroism spectra. *J. Mol. Biol.* **225**, 1075–1093.
41. Shi, Z., Olson, C. A., Rose, G. D., Baldwin, R. L. & Kallenbach, N. R., II (2002). Polyproline structure in a sequence of seven alanine residues. *Proc. Natl Acad. Sci. USA*, **99**, 9190–9195.
42. Kudva, Y. C., Hiddinga, H. J., Butler, P. C., Mueske, C. S. & Eberhardt, N. L. (1997). Small heat shock proteins inhibit *in vitro* A beta(1–42) amyloidogenesis. *FEBS Letters*, **416**, 117–121.
43. Petrosian, S. A. & Makhatadze, G. I. (2000). Contribution of proton linkage to the thermodynamic stability of the major cold-shock protein of *Escherichia coli* CspA. *Protein Sci.* **9**, 387–394.
44. Snyder, S. W., Ladror, U. S., Wade, W. S., Wang, G. T., Barrett, L. W., Matayoshi, E. D. *et al.* (1994). Amyloid-β aggregation: selective inhibition of aggregation in mixtures of amyloid with different chain lengths. *Biophys. J.* **67**, 1216–1228.
45. Perrin, D. D. (1963). Buffers of low ionic strength for spectrophotometric pK determinations. *Aust. J. Chem.* **16**, 572–578.
46. Ding, T. T. & Harper, J. D. (1999). *Analysis of amyloid-β assemblies using tapping mode atomic force microscopy under ambient conditions* Amyloid, Prions, and Other Protein Aggregates (Wetzel, R., ed.), vol. 309, pp. 510–525, Academic Press, New York.
47. Marchant, R. E., Kang, I., Sit, P. S., Zhou, Y., Todd, B. A., Eppell, S. J. & Lee, I. (2002). Molecular views and measurements of hemostatic processes using atomic force microscopy. *Curr. Protein Pept. Sci.* **3**, 249–274.
48. Bustamante, C. & Keller, D. (1995). Scanning force microscopy in biology. *Phys. Today*, **48**, 32–39.
49. Stine, W. B., Jr, Dahlgren, K. N., Krafft, G. K. & LaDu, M. J. (2003). *In vitro* characterization of conditions for amyloid-beta peptide oligomerization and fibrillogenesis. *J. Biol. Chem.* **278**, 11612–11622.
50. Harper, J. D., Lieber, C. M. & Lansbury, P. T., Jr (1997). Jr Atomic force microscopic imaging of seeded fibril formation and fibril branching by the

Alzheimer's disease amyloid-beta protein. *Chem. Biol.* **4**, 951–959.
51. Harper, J. D., Wong, S. S., Lieber, C. M. & Lansbury, P. T. (1997). Observation of metastable Aβ amyloid protofibrils by atomic force microscopy. *Chem. Biol.* **4**, 119–125.
52. Chamberlain, A. K., MacPhee, C. E., Zurdo, J., Morozova-Roche, L. A., Hill, H. A., Dobson, C. M. & Davis, J. J. (2000). Ultrastructural organization of amyloid fibrils by atomic force microscopy. *Biophys. J.* **79**, 3282–3293.
53. Wood, S. J., Chan, W. & Wetzel, R. (1996). Seeding of Aβ fibril formation is inhibited by all three isotypes of apolipoprotein E. *Biochemistry*, **35**, 12623–12628.
54. Serpell, L. C., Sunde, M. & Blake, C. C. (1997). The molecular basis of amyloidosis. *Cell. Mol. Life Sci.* **53**, 871–887.
55. Rochet, J. C. & Lansbury, P. T., Jr (2000). Amyloid fibrillogenesis: themes and variations. *Curr. Opin. Struct. Biol.* **10**, 60–68.
56. Rostagno, A., Revesz, T., Lashley, T., Tomidokoro, Y., Magnotti, L., Braendgaard, H. *et al.* (2002). Complement activation in chromosome 13 dementias: similarities with Alzheimer's disease. *J. Biol. Chem.* **277**, 49782–49790.
57. Mahadevan, D., Chattopadhyay, T., Palmer, R. A., O'Brien, R. & Saldanha, J. W. (2001). Predicted fold for the ABri amyloid subunit: a model for amyloidogenesis in familial British dementia. *Protein Pept. Letters*, **8**, 171–178.
58. McParland, V. J., Kad, N. M., Kalverda, A. P., Brown, A., Kirwin-Jones, P., Hunter, M. G. *et al.* (2000). Partially unfolded states of beta(2)-microglobulin and amyloid formation *in vitro*. *Biochemistry*, **39**, 8735–8746.
59. Ratnaswamy, G., Koepf, E., Bekele, H., Yin, H. & Kelly, J. W. (1999). The amyloidogenicity of gelsolin is controlled by proteolysis and pH. *Chem. Biol.* **6**, 293–304.
60. Rostagno, A., Vidal, R., Kaplan, B., Chuba, J., Kumar, A., Elliott, J. I. *et al.* (1999). pH-Dependent fibrillogenesis of a VkappaIII Bence Jones protein. *Br. J. Haematol.* **107**, 835–843.
61. Chiti, F., Bucciantini, M., Capanni, C., Taddei, N., Dobson, C. M. & Stefani, M. (2001). Solution conditions can promote formation of either amyloid protofilaments or mature fibrils from the HypF N-terminal domain. *Protein Sci.* **10**, 2541–2547.
62. Koga, T., Taguchi, K., Kinoshita, T. & Higuchi, M. (2002). pH-Regulated formation of amyloid-like beta-sheet assemblies from polyglutamate grafted polyallylamine. *Chem. Commun. (Camb.)*, 242–243.
63. Lai, Z., Colón, W. & Kelly, J. W. (1996). The acid-mediated denaturation pathway of transthyretin yields a conformational intermediate that can self-assemble into amyloid. *Biochemistry*, **35**, 6470–6482.
64. Hoyer, W., Antony, T., Cherny, D., Heim, G., Jovin, T. M. & Subramaniam, V. (2002). Dependence of alpha-synuclein aggregate morphology on solution conditions. *J. Mol. Biol.* **322**, 383–393.
65. Alonso, D. O., DeArmond, S. J., Cohen, F. E. & Daggett, V. (2001). Mapping the early steps in the pH-induced conformational conversion of the prion protein. *Proc. Natl Acad. Sci. USA*, **98**, 2985–2989.
66. Zurdo, J., Guijarro, J. I., Jimenez, J. L., Saibil, H. R. & Dobson, C. M. (2001). Dependence on solution conditions of aggregation and amyloid formation by an SH3 domain. *J. Mol. Biol.* **311**, 325–340.
67. Alexandrescu, A. T. & Rathgeb-Szabo, K. (1999). An NMR investigation of solution aggregation reactions preceding the missassembly of acid-denatured cold shock protein A into fibrils. *J. Mol. Biol.* **291**, 1191–1206.
68. Khurana, R., Gillespie, J. R., Talapatra, A., Minert, L. J., Ionescu-Zanetti, C., Millett, I. & Fink, A. L. (2001). Partially folded intermediates as critical precursors of light chain amyloid fibrils and amorphous aggregates. *Biochemistry*, **40**, 3525–3535.
69. Kad, N. M., Thomson, N. H., Smith, D. P., Smith, D. A. & Radford, S. E. (2001). β(2)-Microglobulin and its deamidated variant, N17D form amyloid fibrils with a range of morphologies *in vitro*. *J. Mol. Biol.* **313**, 559–571.
70. Tjernberg, L. O., Pramanik, A., Bjorling, S., Thyberg, P., Thyberg, J., Nordstedt, C. *et al.* (1999). Amyloid beta-peptide polymerization studied using fluorescence correlation spectroscopy. *Chem. Biol.* **6**, 53–62.
71. Zhu, M., Souillac, P. O., Ionescu-Zanetti, C., Carter, S. A. & Fink, A. L. (2002). Surface-catalyzed amyloid fibril formation. *J. Biol. Chem.* **277**, 50914–50922.
72. Kelly, J. W. (1998). The environmental dependency of protein folding best explains prion and amyloid diseases. *Proc. Natl Acad. Sci. USA*, **95**, 930–932.
73. Chiti, F., De Lorenzi, E., Grossi, S., Mangione, P., Giorgetti, S., Caccialanza, G. *et al.* (2001). A partially structured species of beta2-microglobulin is significantly populated under physiological conditions and involved in fibrillogenesis. *J. Biol. Chem.* **276**, 46714–46721.
74. Walsh, D. M., Lomakin, A., Benedek, G. B., Condron, M. M. & Teplow, D. B. (1997). Amyloid β-protein fibrillogenesis. *J. Biol. Chem.* **272**, 22364–22372.
75. Jimenez, J. L., Guijarro, J. I., Orlova, E., Zurdo, J., Dobson, C. M., Sunde, M. & Saibil, H. R. (1999). Cryo-electron microscopy structure of an SH3 amyloid fibril and model of the molecular packing. *EMBO J.* **18**, 815–821.
76. Goldsbury, C., Kistler, J., Aebi, U., Arvinte, T. & Cooper, G. J. (1999). Watching amyloid fibrils grow by time-lapse atomic force microscopy. *J. Mol. Biol.* **285**, 33–39.
77. Conway, K. A., Harper, J. D. & Lansbury, P. T. (1998). Accelerated *in vitro* fibril formation by a mutant alpha-synuclein linked to early-onset Parkinson disease. *Nature Med.* **4**, 1318–1320.
78. Holton, J. L., Ghiso, J., Lashley, T., Rostagno, A., Guerin, C. J., Gibb, G. *et al.* (2001). Regional distribution of amyloid-Bri deposition and its association with neurofibrillary degeneration in familial British dementia. *Am. J. Pathol.* **158**, 515–526.
79. Burdick, D., Soreghan, B., Kwon, M., Kosmoski, J., Knauer, M., Henschen, A. *et al.* (1992). Assembly and aggregational properties of synthetic Alzheimer's A4/β amyloid peptide analogs. *J. Biol. Chem.* **267**, 546–554.
80. Narang, H. K. (1980). High-resolution electron microscopic analysis of the amyloid fibril in Alzheimer's disease. *J. Neuropathol. Expt. Neurol.* **39**, 621–631.
81. Merz, P. A., Wisniewski, H. M., Somerville, R. A., Bobin, S. A., Masters, C. L. & Iqbal, K. (1983). Ultrastructural morphology of amyloid fibrils from neuritic and amyloid plaques. *Acta Neuropathol. (Berl.)*, **60**, 113–124.
82. Walsh, D. M., Hartley, D. M., Kusumoto, Y., Fezoui, Y., Condron, M. M., Lomakin, A. *et al.* (1999). Amyloid beta-protein fibrillogenesis. Structure and

biological activity of protofibrillar intermediates. *J. Biol. Chem.* **274**, 25945–25952.
83. Hartley, D. M., Walsh, D. M., Ye, C. P., Diehl, T., Vasquez, S., Vassilev, P. M. *et al.* (1999). Protofibrillar intermediates of amyloid beta-protein induce acute electrophysiological changes and progressive neurotoxicity in cortical neurons. *J. Neurosci.* **19**, 8876–8884.
84. Kamber, B., Hartmann, A., Eisler, K., Riniker, B., Rink, H., Sieber, P. & Rittel, W. (1980). The synthesis of cystine peptides by iodine oxidation of *S*-trityl-cysteine and *S*-acetamidomethyl-cysteine peptides. *Helv. Chim. Acta*, **63**, 899–915.
85. Bodanszky, M. & Bodanszky, A. (1994). The Practice of Peptide Synthesis, 2nd edit., Springer-Verlag, Berlin.
86. Chen, S. & Wetzel, R. (2001). Solubilization and disaggregation of polyglutamine peptides. *Protein Sci.* **10**, 887–891.
87. Perkins, S. J. (1986). Protein volumes and hydration effects. *Eur. J. Biochem.* **157**, 169–180.
88. Philo, J. S. (1997). An improved function for fitting sedimentation velocity data for low-molecular-weight solutes. *Biophys. J.* **72**, 435–444.
89. Sreerama, N., Venyaminov, S. Y. & Woody, R. W. (1999). Estimation of the number of α-helical and β-strand segments in proteins using circular dichroism spectroscopy. *Protein Sci.* **8**, 370–380.
90. Nichols, M. R., Moss, M. A., Reed, D. K., Lin, W. L., Mukhopadhyay, R., Hoh, J. H. & Rosenberry, T. L. (2002). Growth of beta-amyloid(1–40) protofibrils by monomer elongation and lateral association. Characterization of distinct products by light scattering and atomic force microscopy. *Biochemistry*, **41**, 6115–6127.

Edited by P. T. Lansbury Jr

(Received 18 March 2003; received in revised form 29 July 2003; accepted 2 September 2003)

Supplementary Material comprising one Figure is available on Science Direct